MODELING CYCLOADDITION REACTIONS

by

Sesil Agopcan

B.S., Chemistry, Boğaziçi University, 2009

Submitted to the Institute for Graduate Studies in
Science and Engineering in partial fulfillment of
the requirements for the degree of
Master of Science

Graduate Program in Chemistry
Boğaziçi University

2011

To my family

ACKNOWLEDGEMENTS

I wish to express my sincere gratitude to my thesis supervisor Prof. Viktorya Aviyente for her support, patience and guidance.

I wish to appreciate to the members of my committee: Assist. Prof. F. Aylin Konuklar (Istanbul Technical University) and Assist. Prof. Amitav Sanyal (Boğaziçi University) for their valuable advices and comments.

I gratefully acknowledge Prof. Kendall N. Houk (University of California, Los Angeles) for his advices, comments and his scientific guidance during my stay in UCLA.

I thankfully acknowledge TÜBİTAK BİDEB for the financial support during my studies.

I would like to thank to Nihan Çelebi Ölçüm for her advices, contribution to our work and endless support. Also I wish to thank to Melis Çağdaş for her advices and support. I wish to extend my appreciation to all the members of computational chemistry group, especially to Burcu Dedeoğlu, İlke Uğur, Tuğba Furuncuoğlu Özaltın, Gülşah Çifci and Özlem Karahan. I would like to thank the members of the faculty in Boğaziçi University Chemistry Department, especially Hülya Metiner for her helps and patience.

Finally, I also would like to thank to Sayat Çınar for his endless support and love. I would like to express deepest gratitude to my mother & father and to my brother Sarkis Agopcan for their continuous love and support throughout my life.

ABSTRACT

MODELING CYCLOADDITION REACTIONS

In this study, the selectivities in two types of cycloaddition reactions, namely Diels-Alder and 1,3-dipolar cycloadditions are investigated.

In the first part, the diastereoselectivity in the hydrogen bonding assisted Diels-Alder reactions have been investigated by using different chiral dienes with achiral dienophiles with density functional methods. C9-substituted chiral anthracene templates are used to find out the role of chiral substituents and H-bonding on the product distribution ratio. As a the second study in this part, the π-facial selectivity induced by the presence of a chiral auxiliary in 1,4-substituted butadienes has been considered in order to rationalize the role of the chiral substituent on the stereoselectivity.

In the second part, the conjugate addition/intramolecular nitrone dipolar cycloaddition is investigated with the use of density functional theory. The 1,3-dipolar intramolecular cycloaddition reaction of nitrone is analyzed in details. The most stable and energetically favored mechanism is searched for the interconversion of 6,5,5-tricyclic products to the 6,6,5-tricyclic structure which is the core intermediate to synthesize histrionicotoxins.

ÖZET

SİKLOKATILMA TEPKİMELERİNİN MODELLENMESİ

Bu çalışmada, Diels-Alder ve 1,3-dipolar siklokatılmaları olmak üzere iki tip siklokatılma tepkimesinde seçicilikler incelendi.

Birinci kısımda, farklı kiral dien ve akiral dienofiller kullanılarak hidrojen bağı destekli Diels-Alder reaksiyonlarındaki seçicilik Yoğunluk Fonksiyonları Teorisi (DFT) ile incelenmiştir. Kiral sübstituentlerin ve hidrojen bağının ürün dağılım oranlarındaki etkisini bulabilmek için C9-sübstituentli kiral antrasen türevleri kullanılmıştır. Bu kısımda ikinci bir çalışma olarak 1,4-sübstituentli bütadienlerde de aynı reaksiyon modellenerek kiral sübstituentin stereoselektivitedeki etkisi araştırıldı.

Çalışmanın ikinci kısmında, konjuge katılma/moleküliçi nitron dipolar siklokatılma reaksiyonları DFT ile incelendi. Nitronun 1,3-dipolar moleküliçi siklokatılma reaksiyonu araştırıldı. 6,5,5-üçlü halkalı ürünlerin 6,6,5-üçlü halkalı ürüne dönüşümünün gerçekleştirilebileceği en düşük enerjili mekanizmanın bulunması amaçlandı. Sonuç olarak histrionikotoksin adı verilen doğal bir ürünün sentezinde kullanılan 6,6,5-üçlü halkalı yapının yüksek selektivitede elde edilmesi için yöntemler araştırıldı.

TABLE OF CONTENTS

LIST OF FIGURES

LIST OF TABLES

LIST OF SYMBOLS/ABBREVIATIONS

$E^{\ddagger}$	Electronic activation energy
E_c^{VWN}	Vosko-Wilk-Nusair correlation functional
E_x^{exact}	Exact exchange energy
$E_c[\rho]$	Correlation energy
$E_x[\rho]$	Exchange energy
$E_{\sigma\sigma^*}$	Non-covalent contributions to the energy
$G^{\ddagger}$	Gibbs free energy of activation
$J[\rho]$	Coulomb energy
$T[\rho]$	Kinetic energy of interacting electrons
$T_s[\rho]$	Kinetic energy of non-interacting electrons
U_x^{σ}	Exchange energy density
$V_{ee}[\rho(\mathbf{r})]$	Interelectronic interactions
$V_{ext}(\mathbf{r})$	External potential
V_{KS}	Kohn-Sham potential
ΔE_x^{B88}	Becke's gradient correction
ΔE_0	Relative electronic energy at 0 K
ΔE_{0+ZPE}	Sum of the change in electronic energy and zero point energy at 0 K
ΔH_{rxn}	Heat of reaction as electronic energy
$v(r)$	External potential
$\rho(r)$	Electron density
ψi	Kohn-Sham orbitals
B3LYP	Becke-3-parameter Lee-Yang-Parr functional
B88	Becke 88 Exchange Functional
BMK	Boese-Martin for Kinetics
DFT	Density functional theory
HF	Hartree-Fock theory
LDA	Local density approximation
M062X	Empirical exchange-correlation functionals
MPWB1K	Modified Perdew-Wang-Becke 1 Parameter Method for Kinetics

1. INTRODUCTION

Concerted reactions occur without an intermediate. The transition structure involves both bond breaking and bond formation. There are numerous examples of both unimolecular and bimolecular concerted reactions. A particularly important group consists of the concerted pericyclic reactions [1], which are characterized by a continuous reorganization of electrons through cyclic transition structures. The cyclic transition state must correspond to an arrangement of the participating orbitals that can maintain a bonding interaction between the reacting atoms throughout the course of the reaction.

The major classes of pericyclic reactions are cycloaddition reactions, sigmatropic rearrangements and electrocyclic reactions [2]. In cycloaddition reactions two or more unsaturated molecules combine with the formation of a cyclic adduct. In this reaction there is a net reduction of the bond multiplicity. Sigmatropic rearrangements involve an intramolecular process in which a σ-bond is broken to form an another σ-bond. Electrocyclic reactions are unimolecular reactions likewise sigmatropic rearrangements, where a π-bond is converted to a σ-bond or vice-versa.

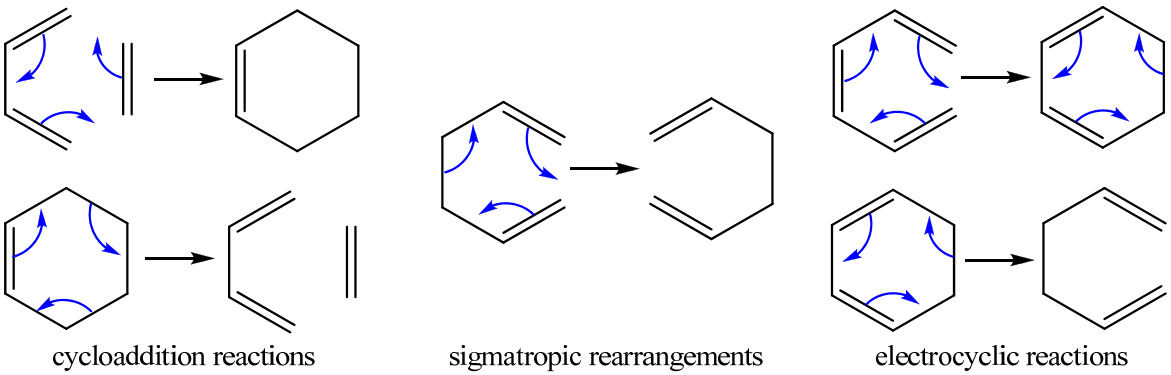

Figure 1.1. Three main classes of pericyclic reactions.

Cycloaddition reactions involve the combination of two molecules to form a new ring. Concerted pericyclic cycloadditions involve reorganization of the π-electron systems of the reactants to form two new σ-bonds [3]. The most important type of the concerted

cycloaddition reactions is the Diels-Alder reaction which consists of a diene and an alkene derivative called dienophile which form a cyclohexene. Another important type of [2+4] cycloaddition is 1,3-dipolar cycloaddition that involve heteroatomic systems that have four π-electrons.

1.1. The Diels-Alder Reactions

The Diels-Alder reaction is one of the most useful synthetic reactions of the construction of the cyclohexane framework. Four contiguous stereogenic centers are created in a single operation, with relative stereochemistry being defined by the usual endo favoring transition state [4].

Orbital symmetry considerations provide a fundamental insight into the electronic nature of the cycloaddition reactions and allow us to see that some of the transition state structures are electronically favorable, whereas others are not [4]. A useful molecular orbital model for analyzing pericyclic reactions has been proposed by Kenichi Fukui. This frontier-orbital approach is based on the assumption that bonds are formed by a flow of electrons from the highest occupied molecular orbital (HOMO) of one reactant or participating bond to the lowest unoccupied molecular orbital (LUMO) of another reactant or bond.

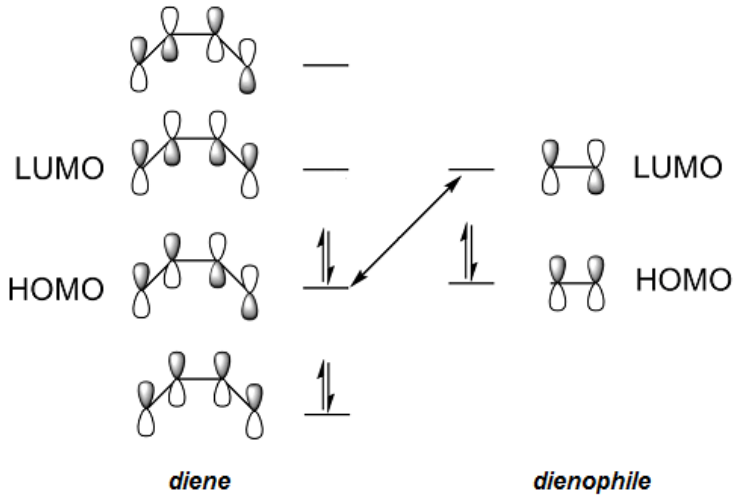

Figure 1.2. Frontier molecular orbital interaction of butadiene and ethylene in Diels-Alder reaction.

The diene and substituted *dienophile* approach each other in parallel planes. For most systems, regioselectivity and stereoselectivity are consistent with a concerted process. This stereospecificity has been demonstrated with many substituted dienes and alkenes and also holds for the simplest possible example of the reaction, ethene with butadiene, as demonstrated by isotopic labeling [5].

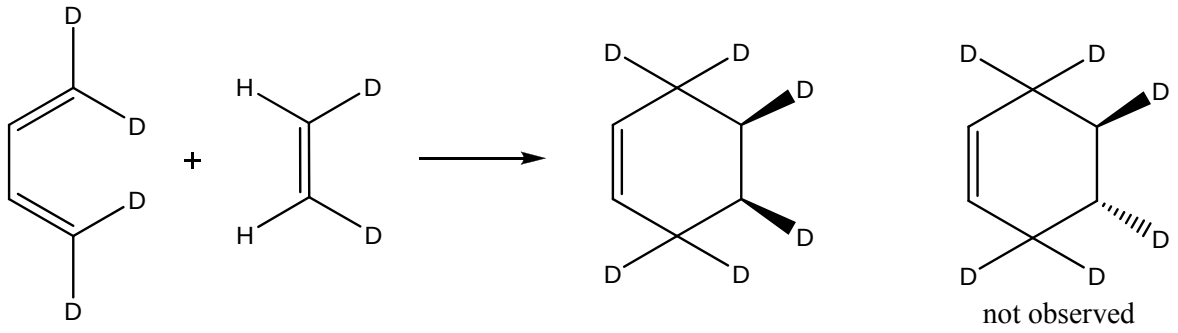

Figure 1.3. Stereospecificity in the Diels-Alder reaction.

For a substituted dienophile, there are two possible stereochemical orientations with respect to the diene. In the *endo* TS the reference substituent on the dienophile is oriented toward the π orbitals of the diene. In the *exo* TS the substituent is oriented away from the π system. The two possible orientations are called *endo* and *exo*, as illustrated in Figure 1.4.

Figure 1.4. Endo and Exo transition state structures for the Diels-Alder reaction.

There are probably several factors that contribute to determining the endo:exo ratio in any specific case, including steric effects, electrostatic interactions, and London dispersion forces [6-7]. Molecular orbital interpretations emphasize secondary orbital interactions

between the π orbitals on the dienophile substituent(s) and the developing π bond of the diene.

Discussions on the reaction mechanism of Diels-Alder cycloadditions had revolved around a choice between a synchronous one-step mechanism, involving a cyclic aromatic transition state and a two-step or two-stage mechanism, involving an intermediate biradical or zwitterion (Figure 1.5). Stepwise passes exist in all pericyclic reactions, and compete with the concerted alternatives.

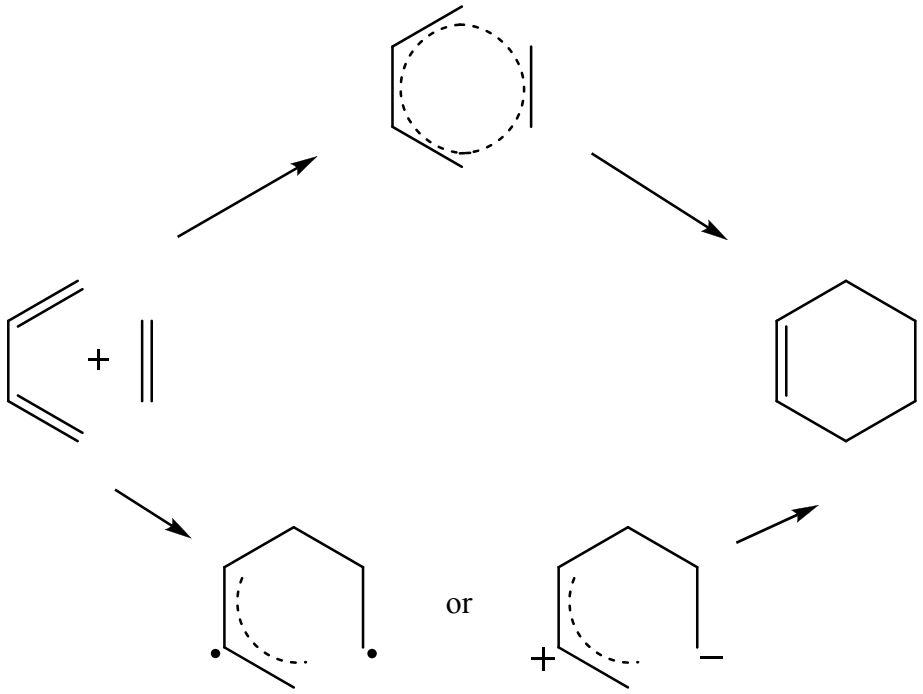

Figure 1.5. One step and two step mechanism of Diels-Alder cycloaddition.

It is assumed that the transition state of such a reaction is very unsymmetrical if one of the new C-C bonds having been almost completely formed (short) while the other is very weak (long). The transition state can then be regarded as a weakly biradical or zwitterion [8]. Therefore, it is not surprising that the most recent developments in the pericyclic reaction chemistry involve the asymmetric versions [9-14, 15-17]. This interest does not seem to decline in the following years, as pericyclic reactions present one of the most powerful approaches to access complex cyclic molecules.

1.2. 1,3-Dipolar Cycloaddition Reactions

1,3-Dipolar cycloadditions are one of the most useful synthetic methods to make stereochemically defined five-membered heterocycles. Nitrones are important 1,3-dipoles that have been the target of catalyzed enantioselective reactions [18-19].

The 1,3-dipolar cycloaddition reaction of nitrones with alkenes is a fundamental reaction in organic chemistry and the available literature on this topic of organic chemistry is vast. In this reaction until three contiguous asymmetric centers can be formed in the isoxazolidine as outlined for the reaction between nitrone and an 1,2-disubstituted alkene. The relative stereochemistry at C-4 and C-5 is always controlled by the geometric relationship of the substituents on the alkene (Figure 1.6) [4].

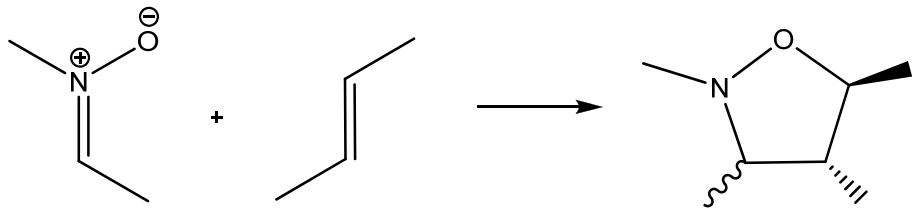

Figure 1.6. Stereochemistry of alkene in 1,3-Dipolar cycloaddition reaction.

The addition of nitrones to alkenes serves both to form a carbon-carbon bond and to introduce oxygen and nitrogen functionality [20]. The products are isoxazolines and the oxygen-nitrogen bond can be cleaved by reduction, leaving both an amino and a hydroxy function in place. A number of imaginative syntheses have employed this strategy. Intramolecular 1,3-dipolar cycloaddition has proven to be especially useful in synthesis.

2 π-electrons of the dipolarophile and 4 electrons of the dipolar compound participate in a concerted, pericyclic shift. The addition is stereoconservative (suprafacial), and the reaction is therefore a [2_s+4_s] cycloaddition similar to the Diels-Alder Reaction. A condition for such a reaction to take place is a certain similarity of the interacting HOMO and LUMO orbitals, depending on the relative orbital energies of both the dipolarophile and the dipole. Electron-withdrawing groups on the dipolarophile normally favor an interaction of the LUMO of the dipolarophile with the HOMO of the dipole that leads to

the formation of the new bonds, whereas electron donating groups on the dipolarophile normally favor the inverse of this interaction.

2. METHODOLOGY

2.1. Density Functional Theory

Kohn-Hohenberg theorems proposed in 1964 [21-22] are the basic idea of the density functional theory (DFT) [23] which is the quantum mechanical approach of the electronic structure of atoms and molecules. The first theorem states that the electron density $\rho(\mathbf{r})$ determines the external potential $V_{\text{ext}}(\mathbf{r})$ and the second theorem introduces the variational principle. As a result, the electron density can be computed variationally and the position of nuclei, energy, wave function and other related parameters can be calculated [23-24].

The electron density is defined as:

$$\rho(x) = N \int \cdots \int |\Psi(x_1, x_2, \cdots, x_n)|^2 dx_1 dx_2 \cdots dx_n \tag{2.1}$$

where x represents both spin and spatial coordinates of electrons.

The electronic energy can be expressed as a functional of the electron density:

$$E[\rho] = \int v(r)\rho(r)dr + T[\rho] + V_{ee}[\rho] \tag{2.2}$$

where $T[\rho]$ is the kinetic energy of the interacting electrons and $V_{ee}[\rho]$ is the interelectronic interaction energy. The electronic energy may be rewritten as

$$E[\rho] = \int v(r)\rho(r)dr + T_s[\rho] + J[\rho] + E_{xc}[\rho] \tag{2.3}$$

with $J[\rho]$ being the coulomb energy, $T_s[\rho]$ being the kinetic energy of the non-interacting electrons and $E_{xc}[\rho]$ being the exchange-correlation energy functional. The exchange-correlation functional is expressed as the sum of an exchange functional $E_x[\rho]$

and a correlation functional $E_c[\rho]$, although it contains also a kinetic energy term arising from the kinetic energy difference between the interacting and non-interacting electron systems. The kinetic energy term, being the measure of the freedom, and exchange-correlation energy, describing the change of opposite spin electrons (defining extra freedom to an electron), are the favorable energy contributions. The Coulomb energy term describes the unfavorable electron-electron repulsion energy and therefore disfavors the total electronic energy [25].

In Kohn-Sham density functional theory, a reference system of independent non-interacting electrons in a common, one-body potential V_{KS} yielding the same density as the real fully-interacting system is considered. More specifically, a set of independent reference orbitals ψ_i satisfying the following independent particle Schrödinger equation are imagined.

$$\left[-\frac{1}{2}\nabla^2 + V_{KS}\right]\psi_i = \varepsilon_i\psi_i \tag{2.15}$$

with the one-body potential V_{KS} defined as

$$V_{KS} = v(r) + \frac{\partial J[\rho]}{\partial \rho(r)} + \frac{\partial E_{xc}[\rho]}{\partial \rho(r)} \tag{2.16}$$

$$V_{KS} = v(r) + \frac{\rho(r')}{|r - r'|}dr' + v_{xc}(r) \tag{2.17}$$

where $v_{xc}(r)$ is the exchange-correlation potential. The independent orbitals ψ_i are known as Kohn-Sham orbitals and give the exact density by

$$\rho(r) = \sum_i^N |\psi_i|^2 \tag{2.18}$$

if the exact form of the exchange-correlation functional is known. However, the exact form of this functional is not known and approximate forms are developed starting

with the local density approximation (LDA). This approximation gives the energy of a uniform electron gas, i. e. a large number of electrons uniformly spread out in a cube accompanied with a uniform distribution of the positive charge to make the system neutral. The energy expression is

$$E[\rho] = T_s[\rho] + \int \rho(r)v(r)dr + J[\rho] + E_{xc}[\rho] + E_b \tag{2.19}$$

where E_b is the electrostatic energy of the positive background. Since the positive charge density is the negative of the electron density due to uniform distribution of particles, the energy expression is reduced to

$$E[\rho] = T_s[\rho] + E_{xc}[\rho] \tag{2.20}$$

$$E[\rho] = T_s[\rho] + E_x[\rho] + E_c[\rho] \tag{2.21}$$

The kinetic energy functional can be written as

$$T_s[\rho] = C_F \int \rho(r)^{5/3} dr \tag{2.22}$$

where C_F is a constant equal to 2.8712. The exchange functional is given by

$$E_x[\rho] = -C_x \int \rho(r)^{4/3} dr \tag{2.23}$$

with C_x being a constant equal to 0.7386. The correlation energy, $E_c[\rho]$, for a homogeneous electron gas comes from the parametrization of the results of a set of quantum Monte Carlo calculations.

The LDA method underestimates the exchange energy by about 10 per cent and does not have the correct asymptotic behavior. The exact asymptotic behavior of the exchange energy density of any finite many-electron system is given by

$$\lim_{x\to\infty} U_x^{\sigma} = -\frac{1}{r} \tag{2.24}$$

U_x^{σ} being related to $E_x[\rho]$ by

$$E_x[\rho] = \frac{1}{2}\sum_{\sigma}\int \rho_{\sigma} U_x^{\sigma}\, dr \tag{2.25}$$

A gradient-corrected functional is proposed by Becke

$$E_x = E_x^{LDA} - \beta\sum_{\sigma}\int \rho_{\sigma}^{4/3}\frac{x_{\sigma}^2}{1+6\beta x_{\sigma}\sinh^{-1}x_{\sigma}}\, dr \tag{2.26}$$

where σ denotes the electron spin, $x_{\sigma} = \frac{|\nabla\rho_{\sigma}|}{\rho_{\sigma}^{4/3}}$ and β is an empirical constant (β=0.0042). This functional is known as Becke88 (B88) functional [21].

The adiabatic connection formula connects the non-interacting Kohn-Sham reference system (λ=0) to the fully-interacting real system (λ=1) and is given by

$$E_{xc} = \int_0^1 U_{xc}^{\lambda} d\lambda \tag{2.27}$$

where λ is the interelectronic coupling-strength parameter and U_{xc}^{λ} is the potential energy of exchange-correlation at intermediate coupling strength. The adiabatic connection formula can be approximated by

$$E_{xc} = \frac{1}{2}E_x^{exact} + \frac{1}{2}U_{xc}^{LDA} \tag{2.28}$$

since $U_{xc}^{0} = E_x^{exact}$, the exact exchange energy of the Slater determinant of the Kohn-Sham orbitals, and $U_{xc}^{1} = U_{xc}^{LDA}$ [22].

The closed shell Lee-Yang-Parr (LYP) correlation functional [**26**] is given by

$$E_c = -a\int \frac{1}{1+d\rho^{-1/3}}\left\{\rho + b\rho^{-2/3}\left[C_F\rho^{5/3} - 2t_w + (\frac{1}{9}t_w + \frac{1}{18}\nabla^2\rho)\right]e^{-c\rho^{-1/3}}\right\}dr \quad (2.29)$$

where

$$t_w = \frac{1}{8}\frac{|\nabla\rho(r)|^2}{\rho(r)} - \frac{1}{8}\nabla^2\rho \quad (2.30)$$

The mixing of LDA, B88, E_x^{exact} and the gradient-corrected correlation functionals to give the hybrid functionals [**27**] involves three parameters.

$$E_{xc} = E_{xc}^{LDA} + a_0\left(E_x^{exact} - E_x^{LDA}\right) + a_x\Delta E_x^{B88} + a_c\Delta E_c^{non-local} \quad (2.31)$$

where ΔE_x^{B88} is the Becke's gradient correction to the exchange functional. In the B3LYP functional, the gradient-correction ($\Delta E_c^{non-local}$) to the correlation functional is included in LYP. However, LYP contains also a local correlation term which must be subtracted to yield the correction term only.

$$\Delta E_c^{non-local} = E_c^{LYP} - E_c^{VWN} \quad (2.32)$$

where E_c^{VWN} is the Vosko-Wilk-Nusair correlation functional, a parametrized form of the LDA correlation energy based on Monte Carlo calculations. The empirical coefficients are a_0=0.20, a_x=0.72 and a_c=0.81 [28].

2.2. Continuum Solvation Models

Continuum solvation models are the most efficient way to include condensed-phase effects into quantum mechanical calculations [29]. Advantage of these models is that they decrease the number of the degrees of freedom of the system by describing them in a

continuous way, usually by means of a distribution function [30-31]. In continuum solvation models, the solvent is represented as a polarizable medium characterized by its static dielectric constant ε and the solute is embedded in a cavity surrounded by this dielectric medium. The total solvation free energy is defined as

$$\Delta G_{solvation} = \Delta G_{cavity} + \Delta G_{dispersion} + \Delta G_{electrostatic} + \Delta G_{repulsion} \quad (2.33)$$

where ΔG_{cavity} is the energetic cost of placing the solute in the medium. Dispersion interactions between solvent and solute are expressed as $\Delta G_{d;spersion}$ which add stabilization to solvation free energy. $\Delta G_{electrostatic}$ is the electrostatic component of the solute-solvent interaction energy. $\Delta G_{repulsion}$ is the exchange solute-solvent interactons not included in the cavitation energy.

The central problem of continuum solvent models is the electrostatic problem described by the general Poisson equation:

$$-\vec{\nabla}\left[\varepsilon(\vec{r})\nabla\vec{V}(\vec{r})\right] = 4\pi\rho_M(\vec{r})$$

simplified to

$$-\nabla^2 V(\vec{r}) = 4\pi\rho_M(\vec{r}) \text{ within } C \quad (2.34)$$

$$-\varepsilon\nabla^2 V(\vec{r}) = 0 \text{ outside } C \quad (2.35)$$

where C is the portion of space occupied by cavity, ε is dielectric function, V is the sum of electrostatic potential V_M generated by the charge distribution ρ_M and the reaction potential V_R generated by the polarization of the dielectric medium:

$$V(\vec{r}) = V_M(\vec{r}) + V_R(\vec{r}) \quad (2.36)$$

Polarizable Continuum Model (PCM) belongs to the class of polarizable continuum solvation models [32]. In PCM, the solute is embedded in a cavity defined by a set of

spheres centered on atoms (sometimes only on heavy atoms), having radii defined by the van der Waals radius of the atoms multiplied by a predefined factor (usually 1.2). The cavity surface is then subdivided into small domains (called tesserae), where the polarization charges are placed. There are three different approaches to carry out PCM calculations. The original method is called Dielectric PCM (D-PCM), the second model is the Conductor-like PCM (C-PCM) [33] in which the surrounding medium is modeled as a conductor instead of a dielectric, and the third one is an implementation whereby the PCM equations are recast in an integral equation formalism (IEF-PCM).

3. AIM OF THE STUDY

This study is composed of two parts which are mainly about the cycloaddition reactions.

In the first study, diastereoselectivity in the hydrogen bonding directed Diels-Alder reactions of chiral dienes with achiral dienophiles is investigated. C9-substituted chiral anthracene templates (R=(CH_3)(OCH_3)(H), R=(CH_3)(OH)(H), R=(CH_3)(CH_2CH_3)(H) and R = (-CH_2-C(CH_3)(OCH_3)(H)) are used to rationalize the role of a stereogenic center and H-bonding on the product distribution ratio. The π-facial selectivity induced by the presence of a chiral auxiliary in 1-substituted 1,3-pentadienes (R1 = (CH_3)(OCH_3)(H) and R1 = (CH_3)(OH)(H)) has also been modeled in order to rationalize the role of the stereogenic center and H-bonding on the stereoselectivity of a straight chain diene. Diastereoselectivities and product distributions are calculated with density functional methods and compared with the experimental results.

The aim of the second study is to investigate the conjugate addition/intramolecular nitrone dipolar cycloaddition with the use of density functional theory. The mechanism of 1,3-dipolar intramolecular cycloaddition reaction of nitrone is analyzed in details.

4. ORIGINS OF THE DIASTEREOSELECTIVITY IN HYDROGEN BONDING DIRECTED DIELS-ALDER REACTIONS OF CHIRAL DIENES WITH ACHIRAL DIENOPHILES

In this study, the origins of diastereoselectivity in the hydrogen bonding assisted Diels-Alder reactions of chiral dienes with achiral dienophiles have been investigated with density functional methods. In the first part, C9-substituted chiral anthracene templates are used to rationalize the role of chiral substituents and H-bonding on the product distribution ratio. The diastereomers are identified according to the stereochemistry around the formed stereocenter on the dienophile attached to C9, as being (R) or (S) respectively. In the second part, the π-facial selectivity induced by the presence of a chiral auxiliary in 1,4-substituted butadienes has been considered in order to rationalize the role of the chiral substituent and H-bonding on the stereoselectivity. In both parts, the product distribution ratios calculated from Boltzmann distributions is in qualitative agreement with the experimental results.

4.1. Introduction

Asymmetric Diels-Alder reaction is among the most powerful and widely utilized processes to access enantiopure six-membered cycles. An exciting progress in the asymmetric Diels-Alder chemistry is the use of chiral dienes as stereodirecting elements to yield cycloadducts with high enantiomeric and diastereomeric excesses [34]. The utilization of chiral dienes opens up the possibility to stereoselectively functionalizes achiral dienophiles by means of a Diels-Alder/retro-Diels-Alder sequence [35].

The Diels-Alder/retro-Diels-Alder strategy involves a binding-transforming-releasing sequence, which can be regarded as a basic mimic to enzymes, nature's complex homochiral templates for stereoselective transformations. The sequence (Figure 4.1) starts with the cycloaddition of the achiral dienophile with the chiral diene template to give a diastereomerically pure cycloadduct [36]. The stereocenters on the cycloadduct allow

enantioselective functionalization of the dienophile subunit, which finally is released in the cycloreversion step.

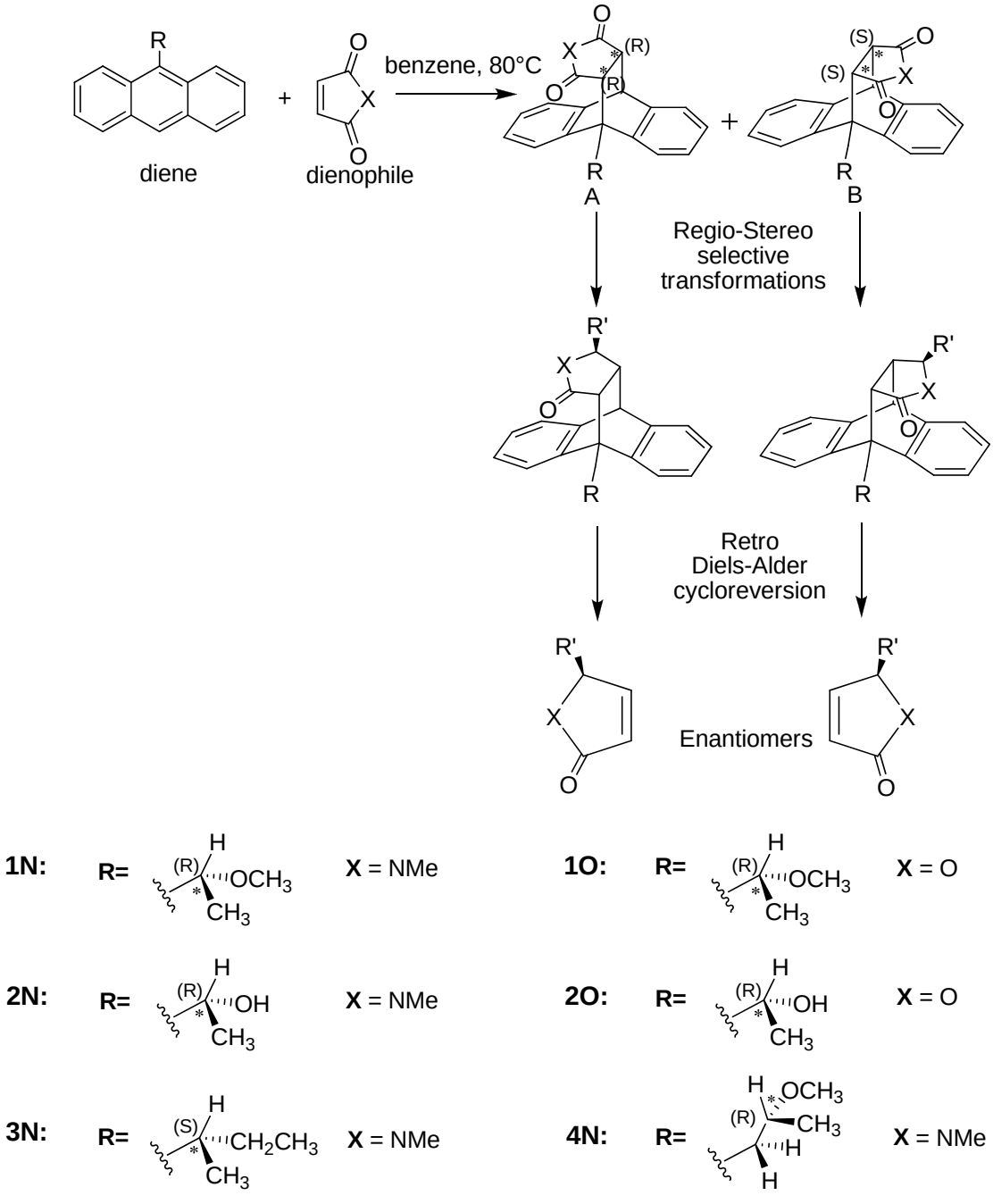

Figure 4.1. Stereoselective Functionalization of the Dienophile Using Chiral Anthracene Template.

An understanding of the key factors that determine the selectivity of the cycloadditions of different chiral dienes with various dienophiles is particularly important for the development of reliable models that explain the origins of the chiral induction.

More recently, Snyder et al. [37-42] and Jones et al. [43-47] have successfully employed chiral 9-substituted anthracene templates for the preparation of α,β-butenolides and α,β-unsaturated lactams with high enantiomeric excess from *N*-methyl maleimide and maleic anhydride.

In this study we investigate (1) the origins of the facial recognition and diastereoselectivity for different chiral diene templates and dienophiles, (2) the importance of the location of the chiral central on the template in the established levels of diastereoselectivity, (3) the effect of a favorable hydrogen bonding interaction between the diene and dienophile in determining the stereochemical outcome of the cycloaddition reaction. We finally apply distortion-interaction [48-54] model to explore the origins of the selectivity of the Diels-Alder reaction.

In the first part, we focus on the reaction of C9-substituted anthracenes as dienes and maleate derivatives as dienophiles to understand the stereochemical nature of the Diels-Alder reaction, the importance of the location of the stereocenter as well as the effect of hydrogen bonding on the stereoselectivity.

In the second part, the mechanistic aspect of the π-facial selectivity will be compared to the selectivity induced by a C9-chiral auxiliary substituted anthracene in terms of barrier heights and in terms of diastereoselectivity; furthermore the effect of H-bonding between the diene and the dienophile will be discussed.

4.2. Methodology

4.2.1. Computational Procedure

Density functional theory was used for all geometry optimizations with Becke's three-parameter hybrid exchange functional and the Lee-Yang-Parr correlation functional

B3LYP/6-31+G(d) level with Gaussian 03 [55-58]. Different hybrid functionals, BMK [59-60], MPWB1K [61], M062X [62-63] have been used with Gaussian 09 [64] to obtain more realistic results. Recent studies show that DFT calculations of the transition states of the above Diels–Alder reactions using the BMK functional, a third-generation hybrid functional tailored for transition state calculations.

Frequency analysis has been performed in order to identify the nature of the stationary points and also to have zero point energies and thermal corrections. Transition states were identified by the presence of a single imaginary vibrational frequency and also IRC calculations have been carried out in order to justify the nature of the reactants and products [65-66].

Solvent effects were evaluated by using the Polarizable Continuum Model (PCM) using the integral equation formalism variant (IEFPCM) with the radii bondi cavity model [67-68]. Benzene is used as a solvent to reproduce the experimental conditions (ε = 2.2706). We used the ideal gas approximation and assumed T = 298.15 K and 1 atm (gas phase) or 1 M concentration (solution). The computation of free energies of activation in solution was done according to typical procedures based on thermodynamic cycles. Accordingly, solvation free energies include a correction to account for change in reference state (This change is RT ln(24.5) and 1.89 kcal/mol at 298.15 K) [69-70].

The conformational analyses for all species were performed by using the PM3 method in Spartan`08 and the conformers within 3 kcal/mol energy range were optimized with B3LYP/6-31+G(d) and BMK/6-31+G(d).

Gibbs free energies in gas phase and in benzene at the B3LYP/6-31+G(d) level are taken account in the study. The population of the diastereomers has been evaluated by using the Boltzmann distribution at 80°C for the first part and at room temperature for the second part. In Boltzmann distribution equation:

$$\frac{n_b}{n_a} = e^{-\frac{\Delta G}{RT}} \qquad (3.1)$$

ΔG is the energy difference between diastereomer A and diastereomer B in terms of Gibbs free energies, R is the Boltzmann constant and T is the temperature.

The transition state energies have been analyzed by decomposing the total electronic energy ($E_0^{\ddagger}$) into the distortion energy, ($E_{dist}^{\ddagger}$) and interaction energy ($E_{int}^{\ddagger}$) as shown in Figure 4.2 by using distortion-interaction model [48-54].

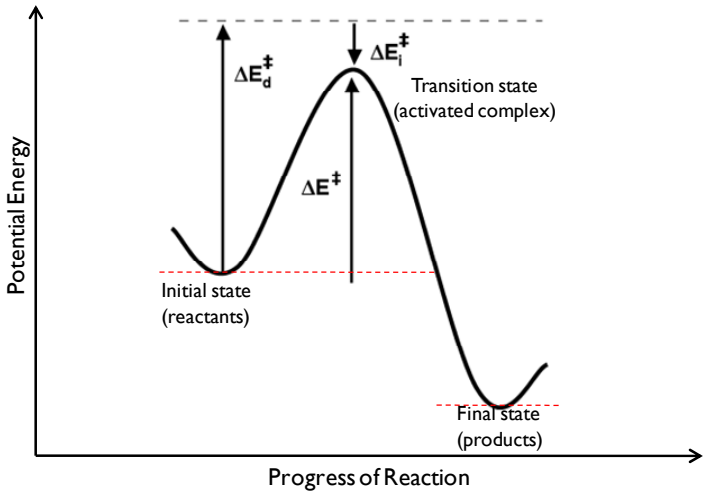

Figure 4.2. Activated Complex Theory and Distortion-Interaction Model.

The strain is the energy associated with deforming the fragments from their equilibrium geometry to the geometry they acquire in the complex. The energy associated with $\Delta E_{int}^{\ddagger}$ is the interaction energy between these deformed fragments in the final geometry [71].

$$\Delta E_0^{\ddagger} = \Delta E_{dist}^{\ddagger} + \Delta E_{int}^{\ddagger} \qquad (3.2)$$

4.3. Results and Discussion

4.3.1. C9-substituent and H-bonding Effect on Diels-Alder Reactions of Anthracenes Derivatives

4.3.1.1. Conformational Analysis of the Reactants. The reactions of C9-substituted anthracenes and maleate derivatives are modeled and explored. The conformational

analyses of the anthracene derivatives are performed. The most stable conformations of the reactants have been located (Table 4.1). In these structures anthracene rings are completely planar.

In the reactants *1* and *2*, the oxygen group (-OMe and –OH) stands far from the anthracene because of steric repulsion of the bulky groups. In the best conformations hydrogen is the closest group to the anthracene because of low electronic repulsion. In the reactant *3*, two bulky groups stay as far as possible from each other, to reduce the repulsion between them. Finally, in the reactant *4*, the bulky group stays alone at one side by repelling the hydrogens. As the bulky groups are far from each other and stay at different faces of anthracene, energy is lowered.

Table 4.1. Conformational analyses of anthracene derivatives.

Conformation	3D structure
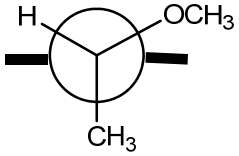 **1**	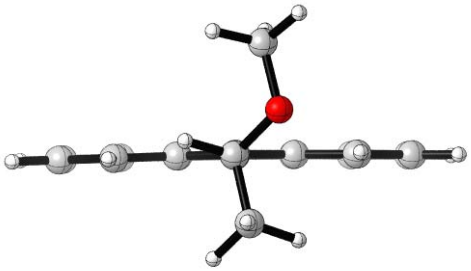
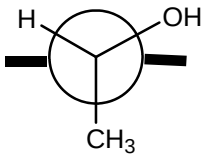 **2**	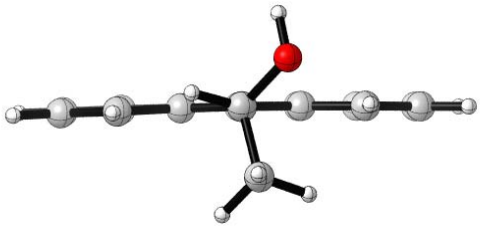

Table 4.1. Conformational analyses of anthracene derivatives. (contd.)

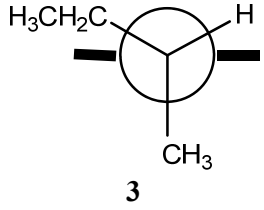 **3**	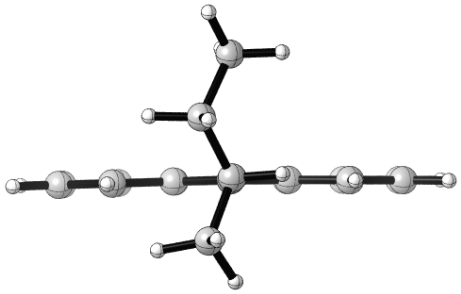
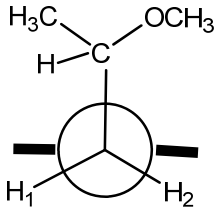 **4**	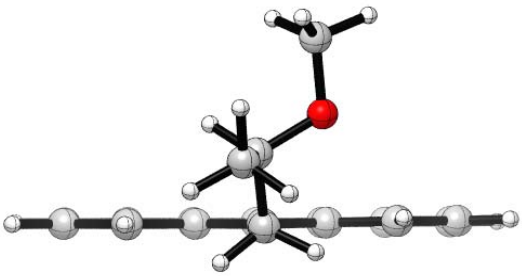

Diels-Alder reactions are modeled with different C-9 substituted anthracene derivatives and maleate derivatives. Diastereoselective addition takes place at the 9 and 10 positions of anthracenes and the stereocenter on these carbons determines the selectivity by being *A* or *B*.

Four different chiral substituents are used on C-9 of the anthracene. To explore the H-bonding effect of the reaction, R_1: $C^*(CH_3)(OCH_3)(H)$ and R_2: $C^*(CH_3)(OH)(H)$ are used and compared with each other. Also to investigate the effect of oxygen on selectivity of the reaction methoxy group is replaced with an ethylene group, R_3: $C^*(CH_3)(CH_2CH_3)(H)$. Lastly, to explore the effect of chiral center position on anthracene, the chiral carbon moved away from the anthracene, R_4: $C^*(\text{-}CH_2\text{-}C(CH_3)(OCH_3)(H)$.

4.3.1.2. Experimental Results. The experimental studies (Table 4.2) carried out by Sanyal, A. et al [37] and Atherton, J. C. C. et al [44-45] have been used in this study to verify our work. Experimental studies on these reactions give 99% diastereoselectivity for the first reaction and much less for the others.

Table 4.2. Experimental studies on Diels-Alder reactions of chiral anthracenes with maleate derivatives. (*The nature of the stereoisomers has not been identified)

Reaction	R	X	conditions	% yield	dr
1N	1	NMe	Benzene, 80°C, 9h	92	>99:1
1O	1	O	Benzene, 80°C, 9h	89	>99:1
2N	2	NMe	Benzene, 80°C, 9h	66	1:1.7
2O	2	O	Toluene, 30°C	65	1:2.1[6b]
3N	3	NMe	Benzene, 80°C, 6h	66	3:2*
4N	4	NMe	Benzene, 80°C, 6h	63	3:2*

4.3.1.3. Conformational Analysis of the Transition States. Model transition states leading to diastereomers *A* and *B* according to their stereocenter on dienophile attached to C9 being R and S respectively for the cycloaddition of MA and NMM to the chiral anthracene is shown in Figure 4.3. By using these 6 approaches, transition state structures are modeled and free energies are calculated at 80°C in the gas phase and also in solvent (benzene) to be able to do a good comparison with experimental results.

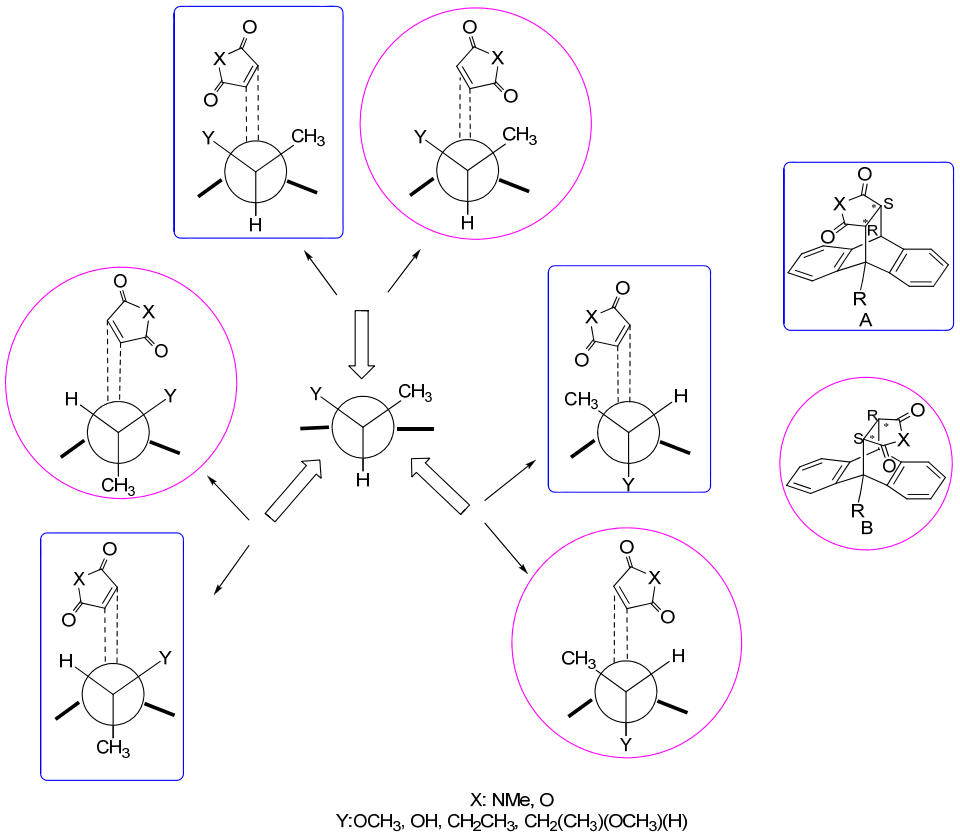

Figure 4.3. Model transition states to diastereomers *A* and *B* for reactions *1* to *4* with *MA* and *NMM*.

The reaction of chiral anthracene derivative with *NMM* is modeled with six different approach of diene to the anthracene as shown in Figure 4.4 and the best *A* (*TS1N-I*) and *B* (*TS1N-IV*) structures are taken account.

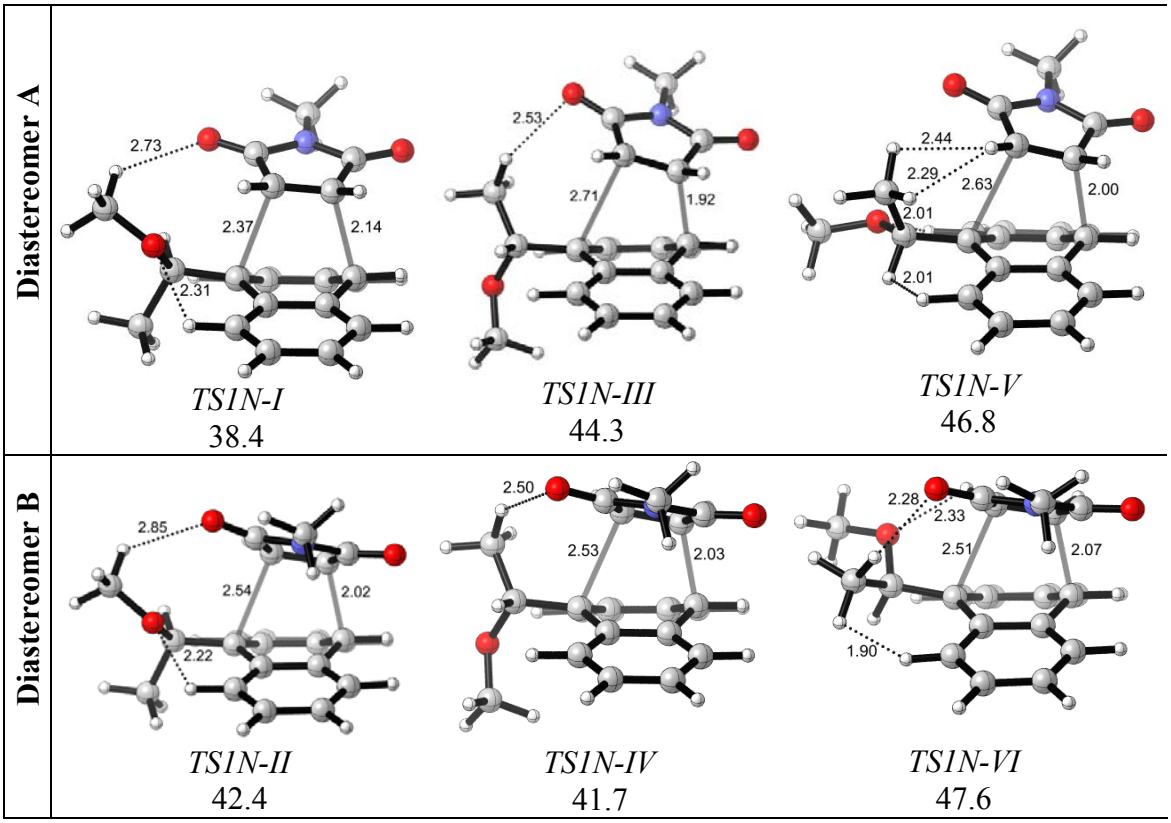

Figure 4.4. Transition state geometries corresponding to reaction 1N (B3LYP/6-31+G(d).

The most stable transition state between methoxy substituted chiral center on C-9 of anthracene and N-methyl maleimide is *TS1N-I* with 38.4 kcal/mol Gibbs free energy in the gas phase. In *TS1N-I* there are two stabilizing O…H interactions between the diene and the dienophile, which causes decrease in energy. One of these interactions, between oxygen of methoxy group on anthracene and hydrogen of *NMM* is absent in the *TS1N-IV*. The most stable transition structures that give *A* (*TS1N-I*) and *B* (*TS1N-IV*) have energy difference 3.3 kcal/mol. This difference is very high and gives rise to good selectivity of the reaction *1N*.

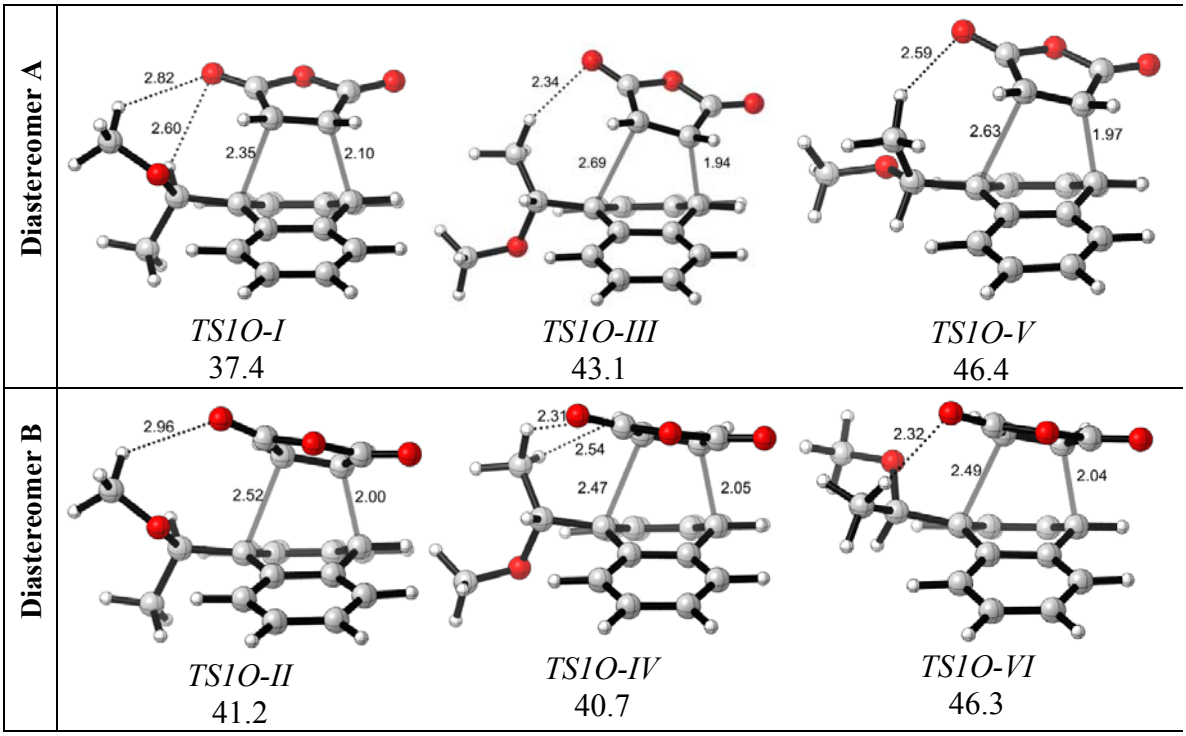

Figure 4.5. Transition state geometries corresponding to reaction 1O (B3LYP/6-31+G(d).

In the reaction *1O* maleic anhydride is used instead of *NMM* with the same anthracene derivative in the reaction *1N* (Figure 4.5). The most stable transition state corresponds to diastereomer *A* like in reaction *1N*. In this reaction the Gibbs free energies are slightly lower than *1N*. *TS1O-I* includes also two stabilizing interaction between the anthracene and *MA*. The interaction between oxygen of the maleic anhydride and the hydrogen of the methoxy group is also present in *TS1O-IV* structure. However another O…H interaction between oxygen of methoxy group and hydrogen of maleic anhydride lacks in *TS1O-IV* because of the anthracene structure in which methoxy group looks down and stays away from the *MA*. The selectivity of reaction *1O* is good because of energy difference between the best diastereomers *A* and *B*.

Reaction *2N* consists of hydroxyl substituted chiral center on C-9 of the anthracene and N-methyl maleimide (*NMM*). The reason why this reaction modeled is to investigate the role of H-bonding in the Diels-Alder reactions. All the six transition structures that give diastereomers *A* and *B* are shown in Figure 4.6.

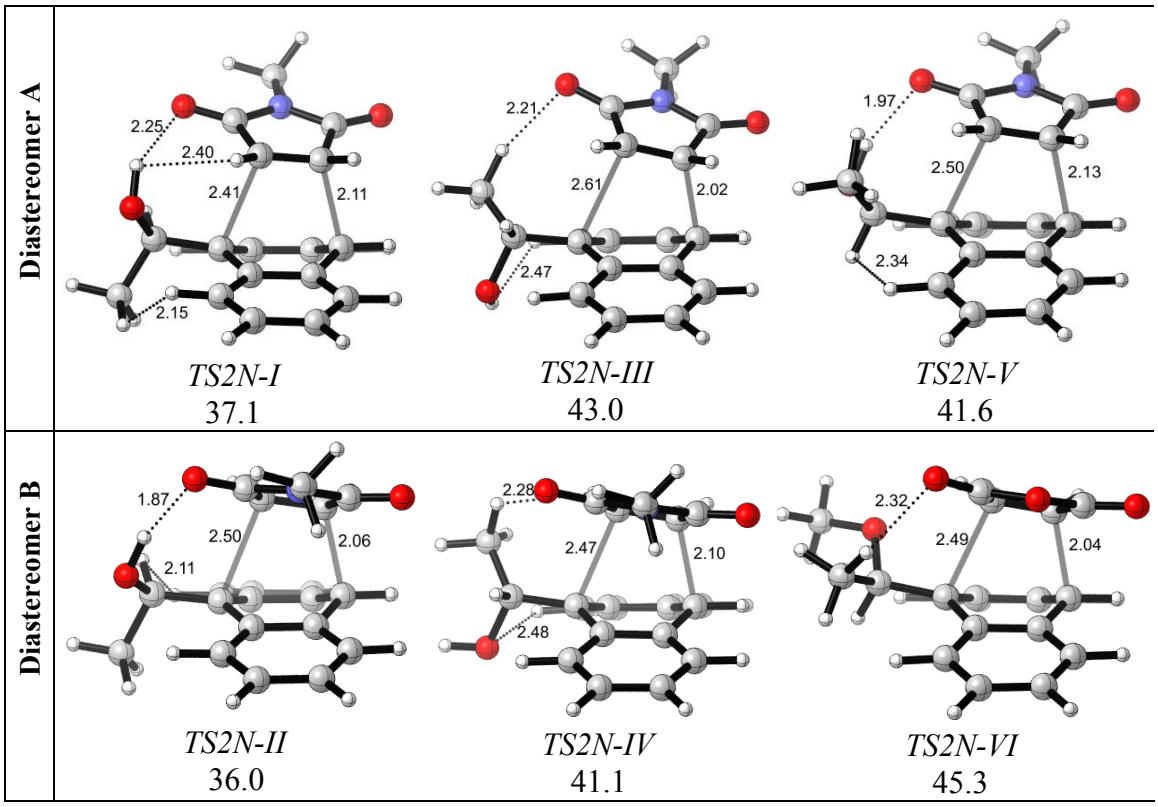

Figure 4.6. Transition state geometries corresponding to reaction *2N* (B3LYP/6-31+G(d).

Both *TS2N-I* and *TS2N-II*, the transition states with the lowest energies include the stronger H-bonding interaction between anthracene and *NMM*. When these two structures are examined it can be concluded that the diastereomer *B* has more H-bonding character because of linearity of O-H…O interaction. This favorable interaction causes lower energy and preference of *B* over *A*. The energy difference between the best diastereomer *A* and *B* is 1.1kcal/mol which results in poor selectivity.

In the reaction *2O*, dienophile *NMM* is replaced with *MA* and the effect of dienophile is investigated. The minimum energy transition state resulting in diastereomer *A*, *TS2O-I*, is 0.2 kcal/mol less stable than *TS2O-II* in the gas phase. Stronger H-bonding interaction in *TS2O-B* favors diastereomer *B*, on the other hand steric hindrance and being more synchronous favors diastereomer *A*. As a result diastereomer *B* slightly dominates on *A* and reaction *2O* gives poor selectivity again (Figure 4.7).

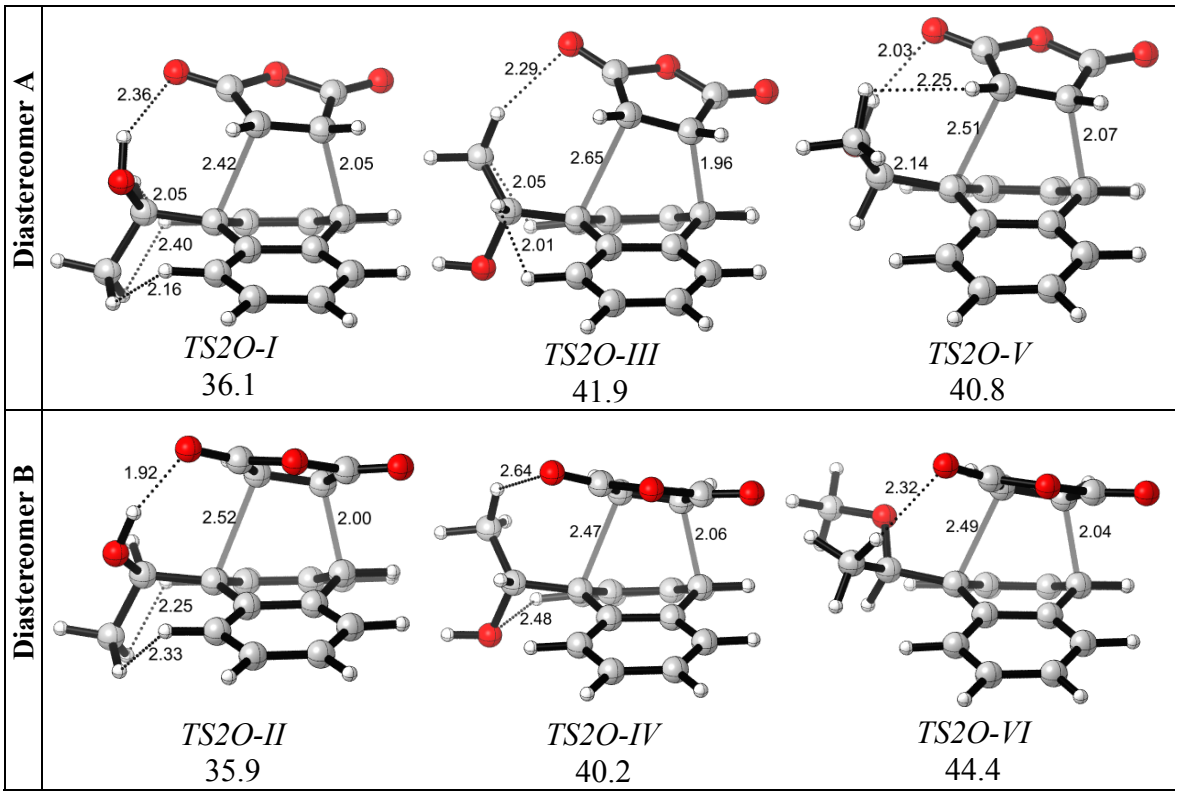

Figure 4.7. Transition state geometries corresponding to reaction *2O* (B3LYP/6-31+G(d).

When the reactions *1* and *2* are compared it can be seen that the energy barriers in reaction *2* are lower than those of reaction *1* because of strong stabilizing H-bonding interactions in *2N* and *2O* which lack in *1N* and *1O*. However the identity of the dienophile -*MA* and *NMM*- has no major role in the stereoselectivities of these reactions.

In the third reaction *3N*, the methoxy group on the chiral center is replaced with an ethyl group to see the effect of oxygen in selectivity of Diels-Alder reactions. In Figure 4.8 the most stable transition state structures are given with the Gibbs free energies in gas phase.

With the replacement of methoxy group with an ethyl group one of the stabilizing interaction that we observed in the reaction *1N* disappears and selectivity between diastereomers *A* and *B* is removed. Also, the Gibbs free energies of reaction *3* are higher than those of reaction *1* because of absence of O…H interactions.

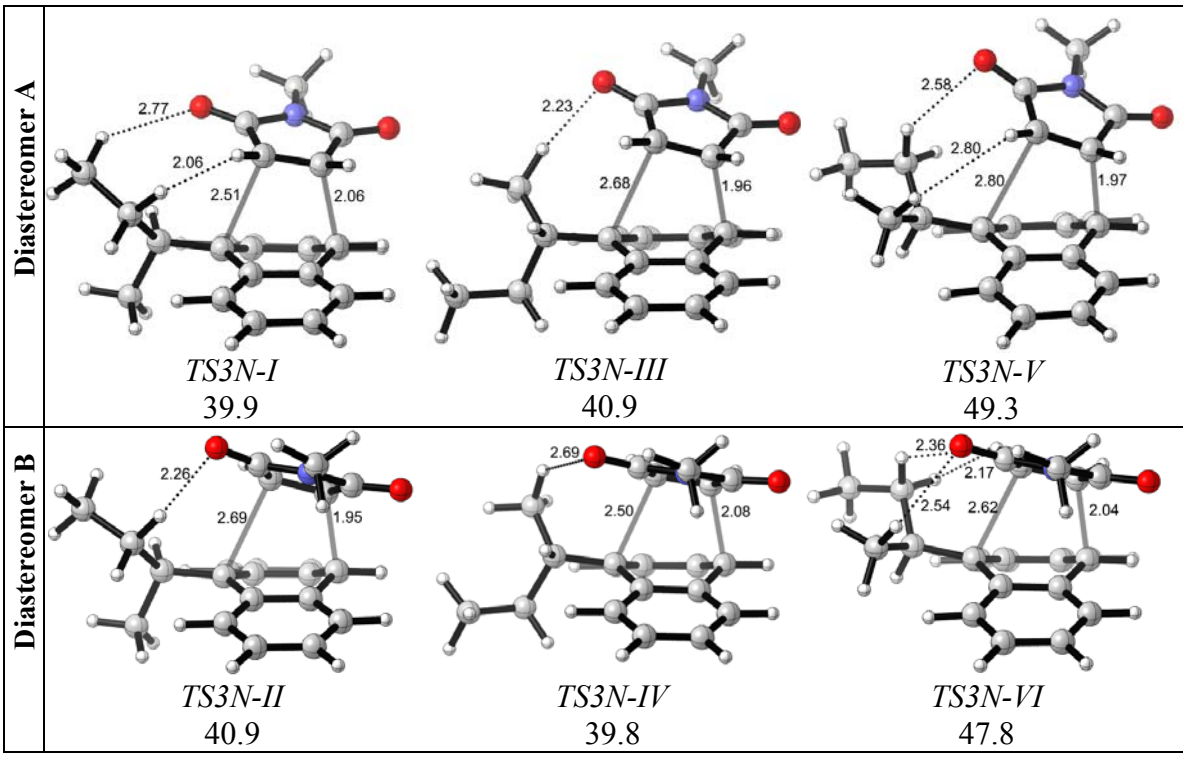

Figure 4.8. Transition state geometries corresponding to reactions *3N* (B3LYP/6-31+G(d).

The reaction between compound *4* in which chiral center is moved one carbon away from the C-9 of the anthracene and *NMM* is shown in Figure 4.9. In this reaction the importance of the position of chiral center on selectivity is investigated.

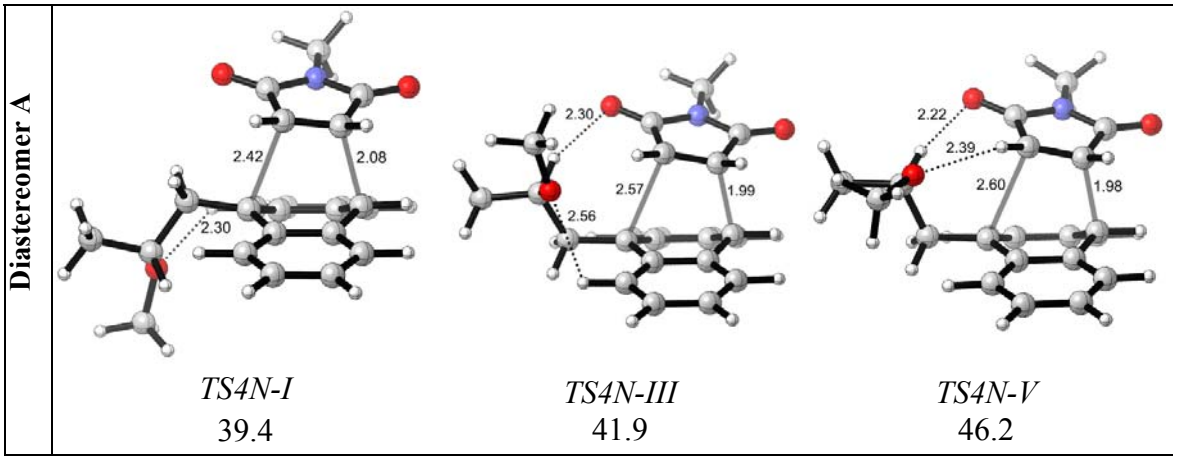

Figure.4.9. Transition state geometries corresponding to reactions *4N* (B3LYP/6-31+G(d).

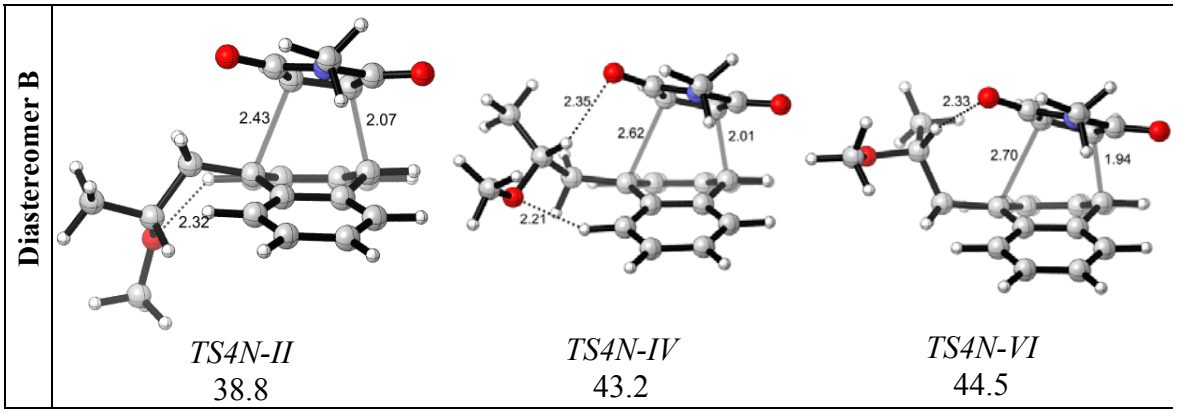

Figure 4.9. Transition state geometries corresponding to reactions *4N* (B3LYP/6-31+G(d). (contd.)

In these reactions the dienophile, *NMM* prefers approach anthracene from the least hindered face, between two hydrogens. Two diastereomers, *TS4N-I* and *TS4N-II* have almost the same structure with no stabilizing interactions. Energies are almost same and the reaction has poor selectivity with slight preference for diastereomer *B*.

The Boltzmann distributions of best diastereomers *A* and *B* are calculated for all reactions between anthracene derivatives and maleate derivatives in gas phase and in benzene as solvent by using Gibbs free energies (Table 4.3). These ratios are compared with the experimental results and are all in agreement with them.

Table 4.3. Diastereomeric ratios for reactions 1, 2, 3 and 4 based on Gibbs free energies (B3LYP/6-31+G(d), BMK/6-31+G(d) in paranthesis and solvent ratios in bold) and dipole moments, μ.

	Diastereomeric Ratio*	**μ**
TS1N-A	0.97 (0.98) - **0.94** [0.99]	1.058
TS1N-B	0.03 (0.02) – **0.06** [0.01]	1.065
TS1O-A	0.97 (0.98) – **0.93** [0.99]	2.144
TS1O-B	0.03 (0.02) – **0.07** [0.01]	2.219
TS2N-A	0.26 (0.26) – **0.27** [0.37]	0.913

Table 4.3. Diastereomeric ratios for reactions 1, 2, 3 and 4 and dipole moments, μ. (contd.)

TS2N-B	0.74 (0.74) – **0.73** [0.63]	1.271
TS2O-A	0.45 (0.47) – **0.38** [0.32]	1.943
TS2O-B	0.55 (0.53) – **0.62** [0.68]	2.578
TS3N-A	0.46 (0.47) – **0.41** [0.40]	1.206
TS3N-B	0.54 (0.53) – **0.59** [0.60]	1.280
TS4N-A	0.34 (0.23) – **0.31** [0.40]	1.724
TS4N-B	0.66 (0.77) – **0.69** [0.60]	1.428

*Experiments are conducted in benzene.[37]

4.3.1.4. Conformational Analysis of the Products. Conformational analysis of the products in each reaction is performed in order to get information about exothermicities of the reactions. The most stable conformations of these products are shown in Figure 4.10.

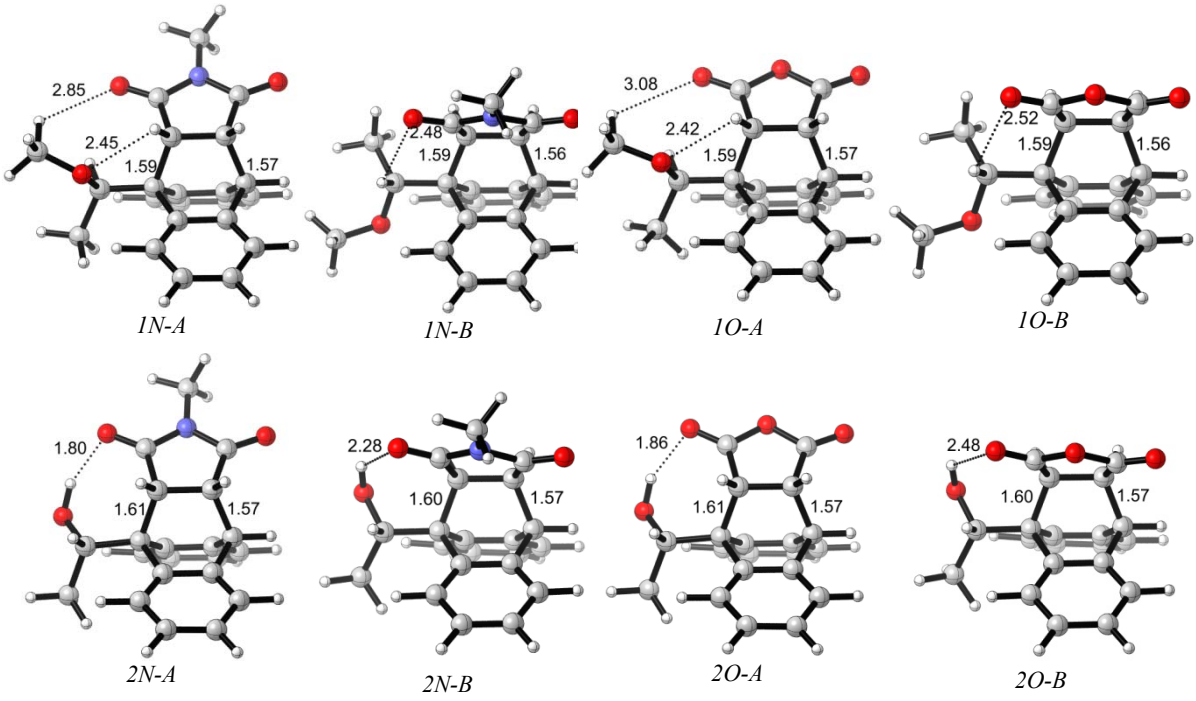

Figure 4.10. Most stable conformations of the products for reactions *1, 2, 3* and *4*.

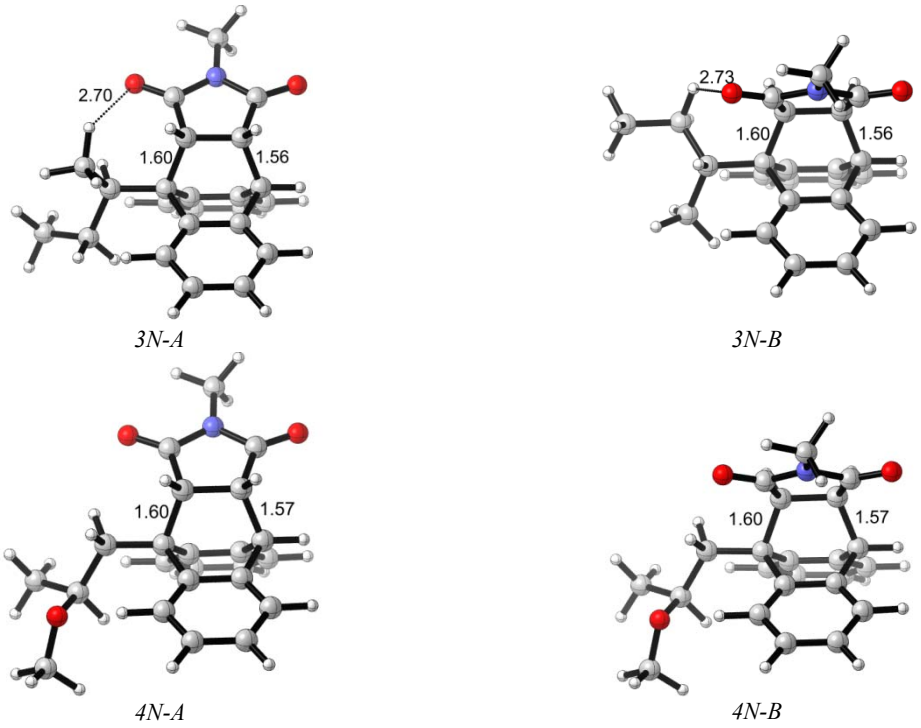

Figure 4.10. Most stable conformations of the products for reactions *1, 2, 3* and *4*. (contd.)

Exothermicities for the reactions *1N, 2N, 1O, 2O, 3N* and *4N* are calculated by using the energies of products and the reactants. These calculations showed that all the reactions are highly exothermic. The effect of H-bonding is not reflected in the exothermicity values therefore the reactions are kinetically controlled. Transition states are for these reactions are reactant-like.

4.3.2. H-Bonding Effect in π Facial Selectivity in Diels-Alder Reactions

The nature of the reactant is one of the important features in the stereoselectivity of the Diels-Alder reaction. Compared to the first part of the study on Diels-Alder reactions, in this part an acyclic diene is used instead of a symmetric anthracene. In this case, instead of observing diastereomer A and B, as in first part, endo/exo stereoselectivity is observed.

4.3.2.1. Experimental Results. Experimental studies by Franck et. al [72] have demonstrated that steric and electronic characteristics of diene and dienophile determines the π-facial selectivity in the reaction. The term *like* used in these reactions describes the

dienophile approach on the *re* face of the double bond with an adjacent R-configurated allylic center, or vice versa.

In the reactions of determination of hydrogen bonding effects on the π-facial selectivity, $(CH_3)(OCH_3)(H)$ and $(CH_3)(OH)(H)$ groups are used on the stereogenic center of the diene and N-phenyl maleimide (NPM) as dienophile as shown in Figure 4.11.

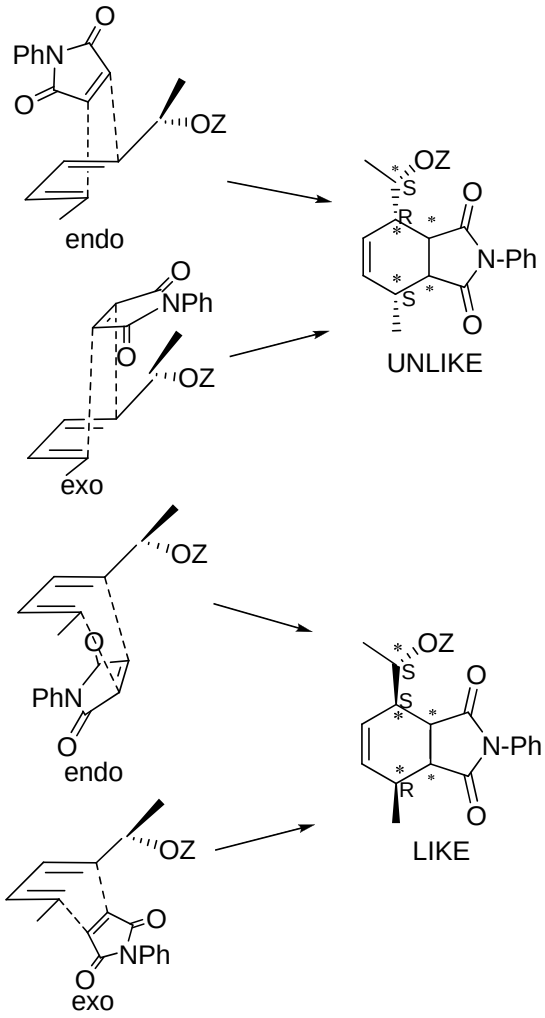

Figure 4.11. Diels-Alder Reaction of 1-substituted 1,3-pentadienes with *NPM*. (*5*:Z=CH_3, *6*:Z=H)

4.3.2.2. Conformational Analysis of the Dienes. The conformational study of the dienes *5* and *6* has revealed that they both exhibit zigzag-like chain structures (Table 4.5).

Table 4.4. Conformations of the dienes *5* and *6*.

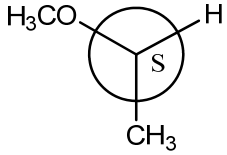 Reactant-5	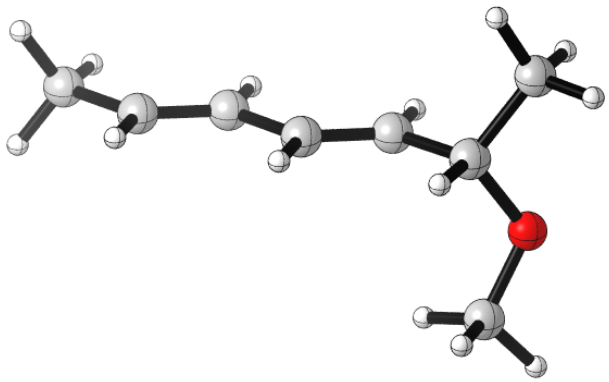
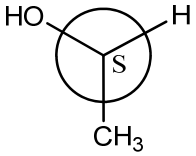 Reactant-6	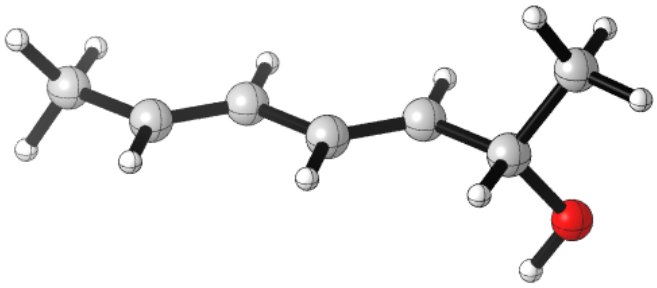

Because of steric reasons the conformation alike to the structure of diene that is shown in Figure 4.11 is not preferred. The dienes have a stereogenic center that has an S stereocenter.

4.3.2.3. Conformational Analysis of the Transition States. The dienophile N-phenyl maleimide (NPM) can approach the diene from either face to yield exo and endo products as shown in Figure 4.11. As a result, in the reaction the products are classified as like-endo, like-exo, unlike-endo and unlike-exo.

The transition state structures are modeled and classified in terms of like/unlike and endo/exo properties. Because of having a stereogenic center, NPM has the possibility to attach to the diene in either two substituents as to the model transition state for first part (Figure 4.3). As a result, six different transition state conformations are obtained for reaction *5* (Figure 4.12 and Figure 4.13) and for reaction *6* (Figure 4.14 and Figure 4.15) that have like and unlike selectivities respectively.

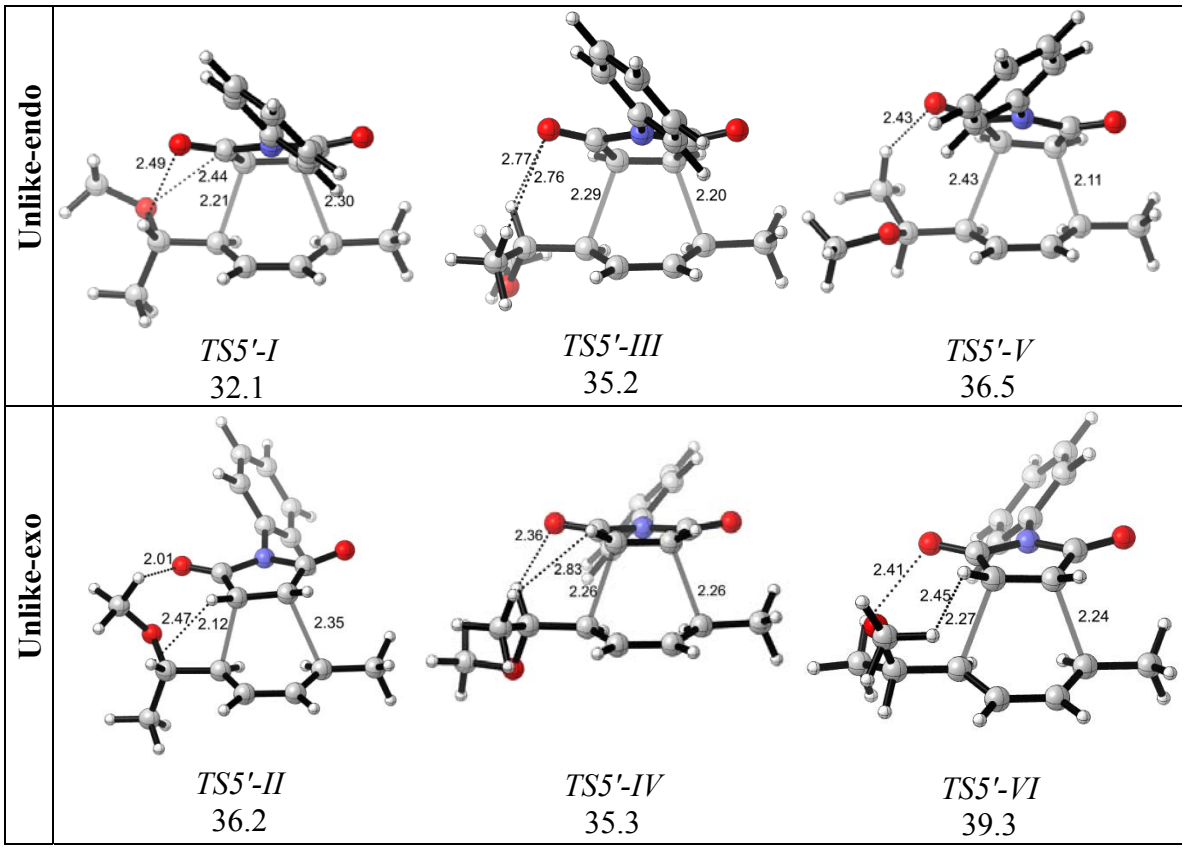

Figure 4.12. Transition state geometries corresponding to reactions *5'-NPM* (B3LYP/6-31+G(d).

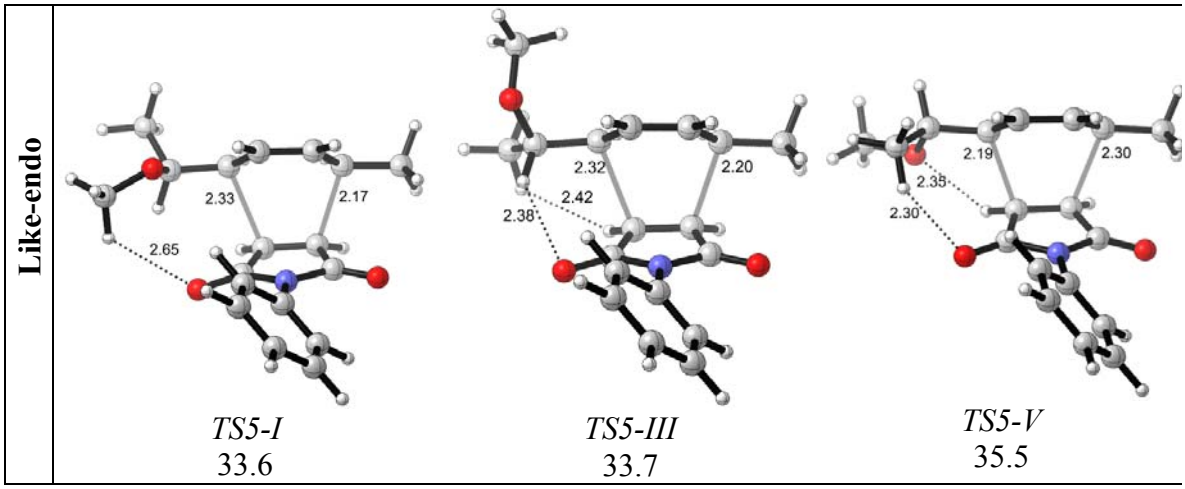

Figure 4.13. Transition state geometries corresponding to reactions *5-NPM* (B3LYP/6-31+G(d).

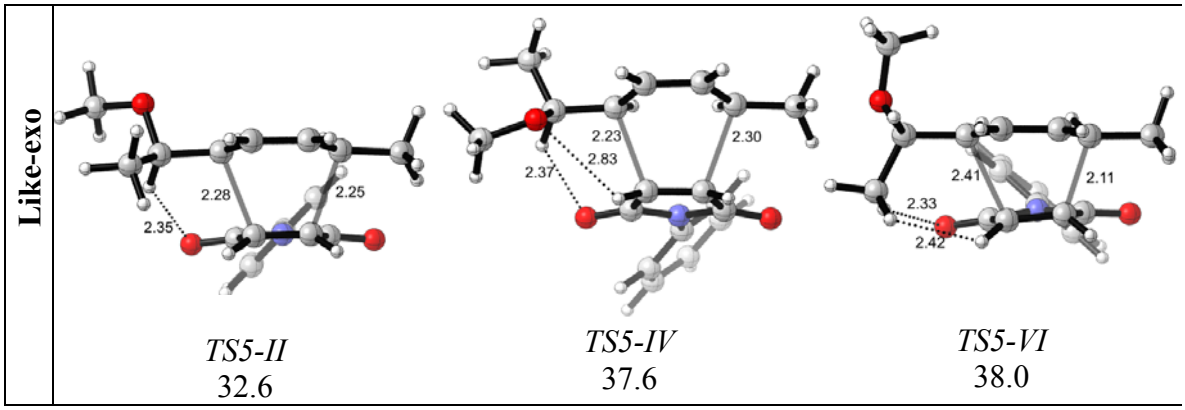

Figure 4.13. Transition state geometries corresponding to reactions *5-NPM* (B3LYP/6-31+G(d). (contd.)

The unlike-endo structure with the lowest barrier corresponds to diastereomer A in reaction *1*. The substituents of dienes *1* and *5* are the same. The dienophile approaches the diene between the hydrogen and the methoxy group, as a result unlike-endo is preferred to like-endo. Both structures are stabilized by CH_3---O interactions. The ratios calculated with Boltzmann distribution by taking into account the Gibbs free energies in gas phase or in solvent (benzene) are in good agreement with the experimental ones (Table 4.6).

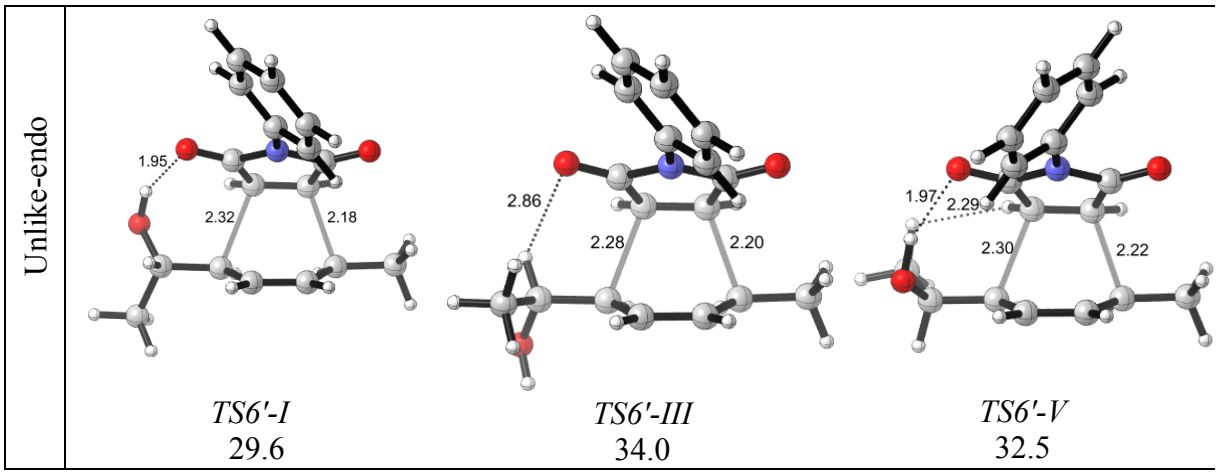

Figure 4.14. Transition state geometries corresponding to reactions *6'-NPM* (B3LYP/6-31+G(d).

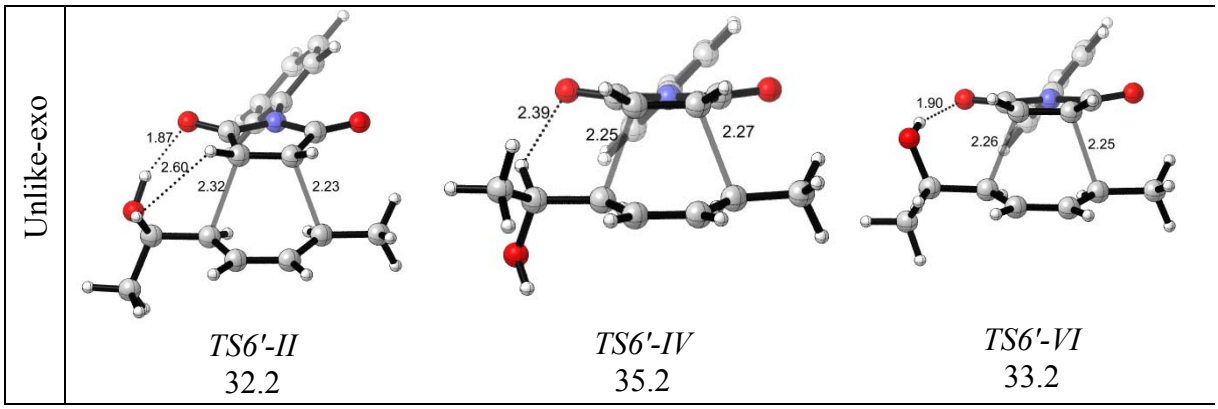

Figure 4.14. Transition state geometries corresponding to reactions *6'-NPM* (B3LYP/6-31+G(d). (contd.)

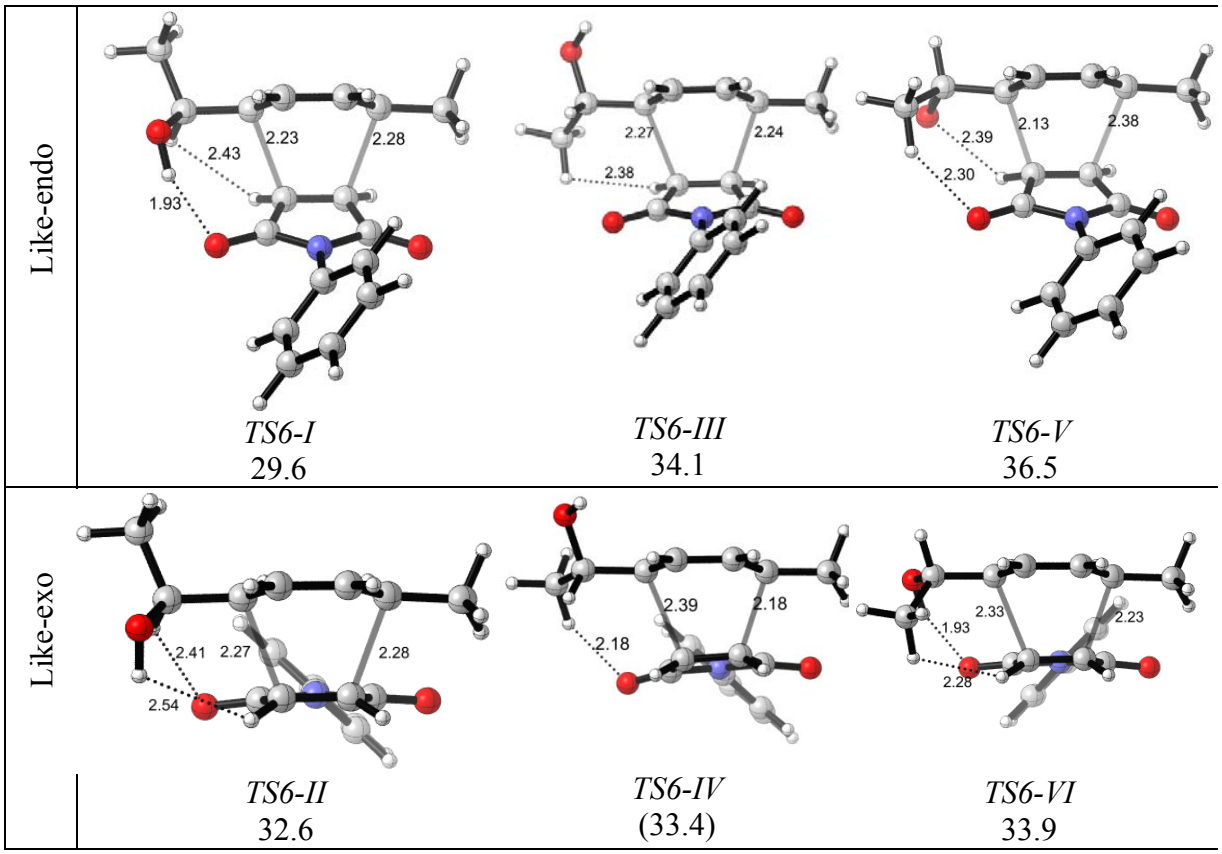

Figure 4.15. Transition state geometries corresponding to reactions *6-NPM* (B3LYP/6-31+G(d).

In reaction of *6* and *NPM*, *TS6'-endo* is like diastereomer A in reaction *2* where the stereogenic carbon bears the same substituents. In *TS6'-I* the dienophile approaches to

diene between hydroxyl group and hydrogen. This approach gives rise to hydrogen bond between the diene and the dienophile with a strong stabilizing interaction and lowering of the energy. The distance between O---H is 1.95Å (Figure 4.14) which is quite well for this interaction. The lowest free energies belong to the structures of like-endo and unlike-endo having the same energy (Table 4.5).

As in reaction *5* with *NPM*, *TS6′-I* is preferred over that of *TS6′-II* because in the later one H-bonding interaction lacks and the most important stabilizing interaction between *6* and *NPM* is lost which causes increase in energy.

In Table 4.5 the calculated diastereomeric ratios are given with the experimental ones. Also the discussion of distortion-interaction model calculated for gas phase activation barriers, distortion energies and interaction energies are given.

Table 4.5. Diastereomeric ratios for reactions *5* and *6* based on Gibbs free energies (B3LYP/6-31+G(d), BMK/6-31+G(d) in paranthesis and solvent ratios in bold) and dipole moments, μ.

	Reaction	Diastereomeric Ratio*	μ
unlike	**TS5′-endo**	0.55 (0.50) - **0.64 (0.60)**	1.192
	TS5′-exo	0.02 (0.00) - **0.03 (0.00)**	0.988
		[0.83]	
like	**TS5-endo**	0.12 (0.01) - **0.12 (0.02)**	1.368
	TS5-exo	0.31 (0.48) - **0.21 (0.38)**	1.091
		[0.17]	
unlike	**TS6′-endo**	0.46 (0.56) - **0.45 (0.53)**	1.206
	TS6′-exo	0.03 (0.01) - **0.03 (0.01)**	1.402
		[0.70]	
like	**TS6-endo**	0.48 (0.43) -**0.50 (0.46)**	1.303
	TS6-exo	0.03 (0.00) - **0.03 (0.00)**	1.391
		[0.30]	

*Experiments are conducted in benzene.[73]

The overlap of secondary orbitals is favored in endo cyclization: in *TS5′-endo* the positive interaction between the orbital with the lone pairs on nitrogen (*NPM*) overlaps with the orbital of same sign on the diene, this stabilizing interaction is lacking in *TS5′-exo*

(Figure 4.16). The secondary orbital interaction (SOI) model has been widely used in explaining the kinetically controlled endo-addition in Diels-Alder reaction [74-82].

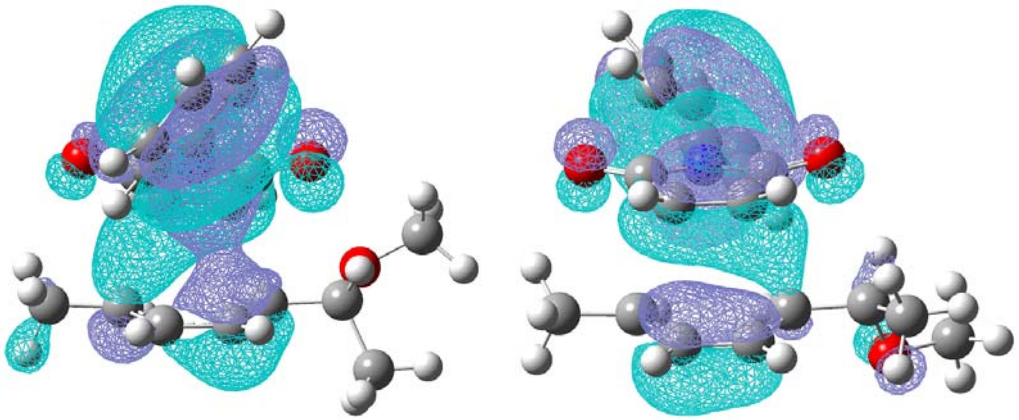

TS5'-endo *TS5'-exo*

Figure 4.16. Highest occupied molecular orbitals for endo and exo transition states in reaction *5'-NPM*.

Frontier molecular orbitals are used to show the primary and secondary orbital interactions in endo and exo cases in Figure 4.17. In these interactions red signs are primary ones and the blue signs for secondary interactions.

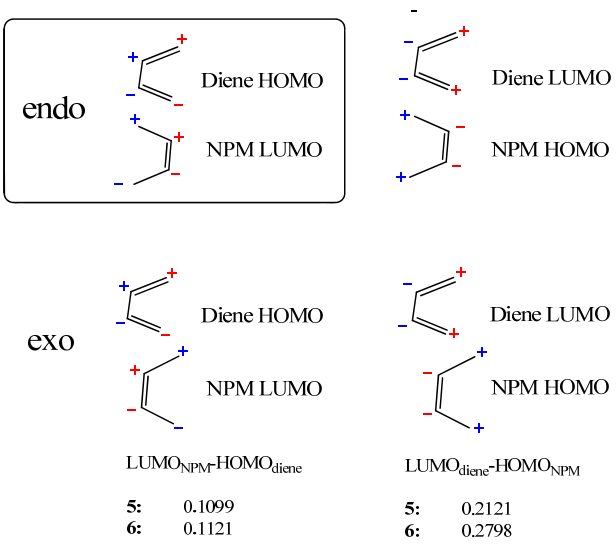

Figure 4.17. Frontier molecular orbitals in Diels-Alder reaction of *5* and *6* with *NPM*.

4.3.2.4. Conformational Analysis of the Products. Conformational analysis of the products in each reaction is performed in order to get information about exothermicities of the reactions. The most stable conformations of these products are shown in Figure 4.18.

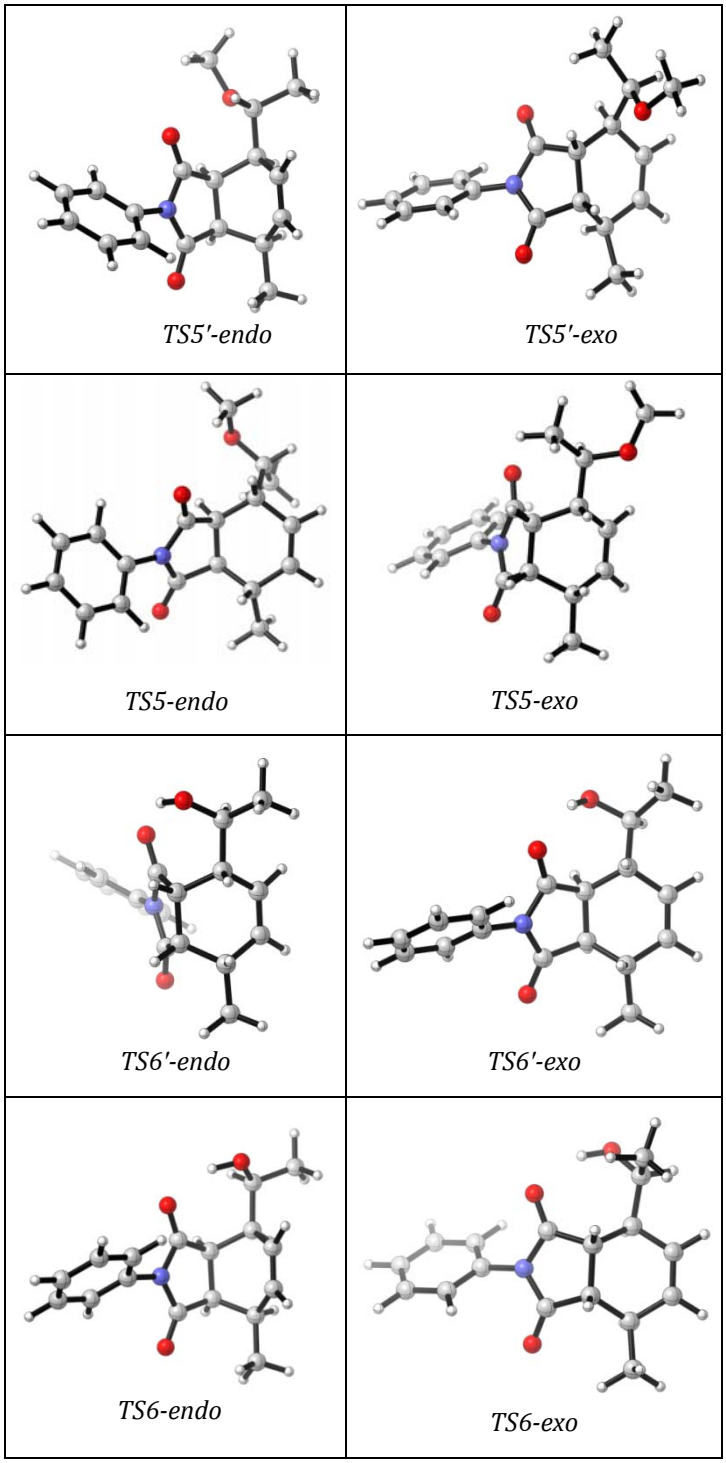

Figure 4.18. Conformations of the products for reaction *5* and *6*.

4.4. Distortion-Interaction Model

Distortion-interaction model is used to find the interaction energies of the reactions. The distortion/interaction model partitions the activation energy ($\Delta E_0^{\ddagger}$) into distortion energy ($\Delta E_{dist}^{\ddagger}$), and interaction energy ($\Delta E_{int}^{\ddagger}$) between distorted fragments, where the former is associated with the strain caused by deforming the individual reactants, and the latter is the favorable interaction between the deformed reactants (Table 4.4) [48-54].

$$\Delta E_0^{\ddagger} = \Delta E_{dist}^{\ddagger} + \Delta E_{int}^{\ddagger}$$

Table 4.6. Gas phase activation barriers ($\Delta E_0^{\ddagger}$), distortion energies ($\Delta E_{dist}^{\ddagger}$), interaction energies ($\Delta E_{int}^{\ddagger}$) (B3LYP/6-31+G(d), in kcal/mol)

	$\Delta E_0^{\ddagger}$	$\Delta E_{dist}^{\ddagger}$	$\Delta E_{int}^{\ddagger}$
TS1N-A	20.2	32.5	-12.3
TS1N-B	23.5	33.6	-10.1
TS1O-A	19.4	35.5	-16.1
TS1O-B	23.0	37.3	-14.3
TS2N-A	17.9	32.3	-14.4
TS2N-B	16.5	31.4	-14.9
TS2O-A	17.7	35.4	-17.7
TS2O-B	16.9	35.2	-18.3
TS3N-A	20.6	31.5	-10.9
TS3N-B	20.7	30.8	-10.1
TS4N-A	21.2	32.5	-11.3
TS4N-B	20.5	32.4	-11.9

Based on the results shown in Table 4.4 the significance of H-bonding interaction in *TS2N* and *TS2O* can be explored by interaction energies. There is larger interaction energy, (18.3 kcal/mol) in the *TS2O-B* than in *TS1O-A* (16.1 kcal/mol). Of the 2.5 kcal/mol difference that favors *TS2O-B* over *TS2O-A* only 0.3 kcal/mol are due to distortion steric interactions with anthracene. The larger interaction energy (2.2 kcal/mol) in *TS2O-B* as compared to *TS1O-A* reflects the stabilization of the latter by hydrogen bonding.

4.5. Conclusions

The substituent effect and the nature of reactants have an important role in determination of stereoselectivities in Diels-Alder reactions. The steric and electronic effects induced by $–OCH_3$ group on the stereogenic center allow efficient stereoselection. H-bonding acquired via –OH substituent on the stereogenic carbon in reaction 2 results in loss of stereospecificity in Diels-Alder reactions. The identity of the dienophile does not seem to play a role in selectivity.

The methodology used (B3LYP/6-31+G(d) and BMK/6-31+G(d)) to determine the Gibbs free energies is merged into the Boltzmann distribution to reproduce the experimental results. The distortion-interaction energies show that diastereoselectivity is mostly governed by interaction energies.

Reactions 5 and 6 with NPM yield primarily the *endo* product as expected based on stabilization through H-bonding and secondary orbital-overlap. Overall, in Diels Alder reactions, the nature of the substituents on the stereogenic center, the proximity of the center to the reactive site play a substantial role in diastereoselectivity.

5. REGIOSELECTIVITY AND STEREOSELECTIVITY IN INTRAMOLECULAR NITRONE 1,3-DIPOLAR CYCLOADDITIONS

In this study, the sequential intramolecular conjugate addition of the oxime is modeled. This addition is followed by intramolecular dipolar cycloaddition of the intermediate nitrone in order to afford a mixture of the isoxazolidines as 6,5,5- and 6,6,5-tricyclic adducts. The tricyclic 6,5,5-adduct can be equilibrated with the epimeric tricyclic 6,5,5-isoxazolidine through a β-elimination/conjugate addition process. Conditions have been developed for the two-step conversion of the ketone into the racemic tricyclic 6,6,5-adduct which is the core precursor of all the known histrionicotoxin alkaloids [83].

5.1. Introduction

In the last 50 years many scientists have drawn special attention to nitrones due to their successful application as building blocks in the synthesis of various natural and biologically active compounds. Nitrones were first prepared by Beckmann in 1890 [84-86] and named as “nitrogen-ketones” by Pfieiffer in 1916 to emphasize their similarity to ketones [87]. Their chemistry is vast but it is dominated by their use as 1,3-dipoles for cycloaddition reactions. In 1960, Huisgen proposed the concept of the 1,3-dipolar cycloaddition reaction in which the accepted concept of the two new bonds occurs as a concerted process [88-89].

The 1,3-dipolar cycloaddition reactions take place between a dipolarophile and a 1,3-dipolar compound that leads to 5-membered (hetero)cycles. 1,3-dipolar cycloaddition reactions can be represented as shown in Figure 5.1. The entity a-b-c is called the 1,3-dipole and d-e is the dipolarophile. The 1,3-dipoles have a π-electron system consisting of two filled and one empty orbital. Each 1,3-dipole has at least one charge-separated resonance structure with opposite charges in a 1,3-relationship which leads to the name 1,3-dipole. The dipolarophiles are typically substituted alkenes or alkynes but the essential characteristic is a π-bond. Therefore other multiply bonded functional groups such as carbonyl, imine, azo, and nitroso can also act as dipolarophiles.

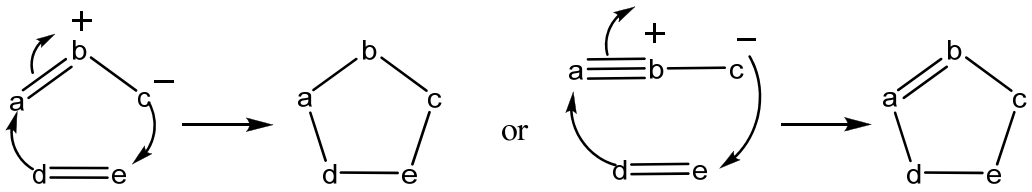

Figure 5.1. Schematic representation of a common 1,3-dipolar cycloaddition reaction.

The most common nitrone 1,3-dipolar cycloaddition reaction is the formation of an isoxazolidines using alkene dipolarophiles, although other multiply bonded systems may also be used. (Figure 5.2)

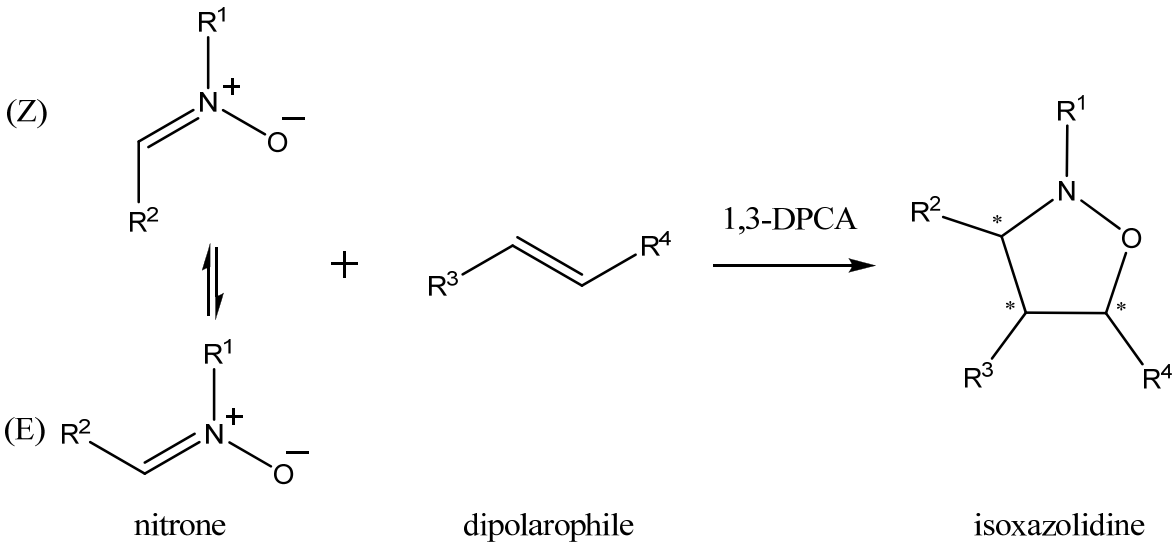

Figure 5.2. Formation of isoxazolidine from nitrone by 1,3-dipolar cycloaddition (1,3-DPCA).

Because of the problem of nitrone isomerization (E/Z), numerous cyclic nitrones have been developed allowing only a single geometry about the C = N double bond. The feature of asymmetric induction through their ability to enforce the cycloaddition reaction at one or other face of the 1,3-dipole, makes cyclic nitrones popular.

Nitrones have found application in the synthesis of a wide range of natural product target types, from sugars and nucleoside analogues, through β-lactams to alkaloids and

other nitrogen heterocyclic natural products [87]. The possible stereochemical control in the pericyclic transition state of the cycloadditions has been a key feature of many of these applications, and has been used to construct acyclic systems.

5.2. Methodology

5.2.1. Computational Procedure

Density functional theory was used with Gaussian 03 [58] and Gaussian 09 [64] program packages. All geometry optimizations were done with Becke's three-parameter hybrid exchange functional and the Lee-Yang-Parr correlation functional B3LYP and also with a hybrid meta-GGA functional, M06-2X [62-63], both with 6-31+G(d) basis set. Higher basis set (6-311+G(d,p)) has been used in accordance with M06-2X functional to obtain more realistic results.

In order to obtain the zero point energies and also thermal corrections for calculations of enthalpies and Gibbs free energies, frequency analysis has been performed. From these frequency analyses single imaginary vibrational frequencies were sought in transition states and also IRC calculations have been carried out in order to justify the nature of the reactants and products [65-66].

The conformational analyses for the reactants and the products were performed by using the PM3 method in Spartan 08 program package. The conformers then were optimized with B3LYP/6-31+G(d) and with M06-2X/6-31+G(d). Single point energies of these conformers were calculated with M06-2X/6-311+G(d,p). The transition state structures were modeled with PM3 then optimized with higher basis sets to find the single imaginary frequency where the transition state is located.

Gibbs free energies in gas phase at two levels (B3LYP/6-31+G(d) and B3LYP/6-31+G(d)//M06-2X/6-311+G(d,p)) are taken account in the study. Relative energies are given with respect to the molecule with the lowest energy. The reactions were conducted also at higher temperature to follow the effect on the formation of products.

5.3. Results and Discussion

In this study, a computational study of kinetic and thermodynamic factors controlling the cycloadduct ratio has been conducted. We also described here the mechanisms and origins of substituent effects on the reaction of synthesis of histrionicotoxins.

During our investigations of the application of nitrone dipolar cycloadditions to the synthesis of histrionicotoxin alkaloids, the Holmes group discovered a series of regio- and stereochemical interconversions among the isomeric cycloadducts [90-94]. The synthesis [95] of histrionicotoxin, *7* (Figure 5.3) involves the key 6,6,5-tricyclic intermediate *6*, obtained from a symmetrical ketone *1*. The crucial intermediate, *6* is the thermodynamically-favored cycloadduct from the *C*-alkenylnitrone *3*, which is produced from an oxime**,** *2***.**

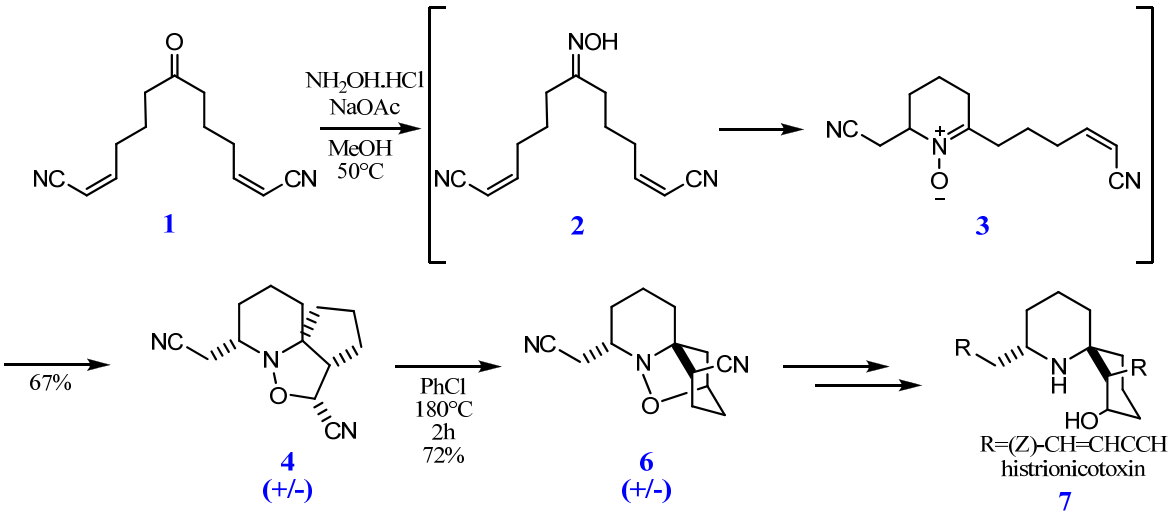

Figure 5.3. Intramolecular nitrone 1,3-dipolar cycloaddition route to the 6,6,5-adduct *6***.**

The cycloaddition of *3* at 50 °C leads selectively to the 6,5,5 tricycle *4*, with smaller amounts of *6* and an epimeric 6,5,5 tricycle, *5*. The mixture of tricycles is thermally isomerized to *6* upon heating in chlorobenzene at 180 °C as shown in Figure 5.4.

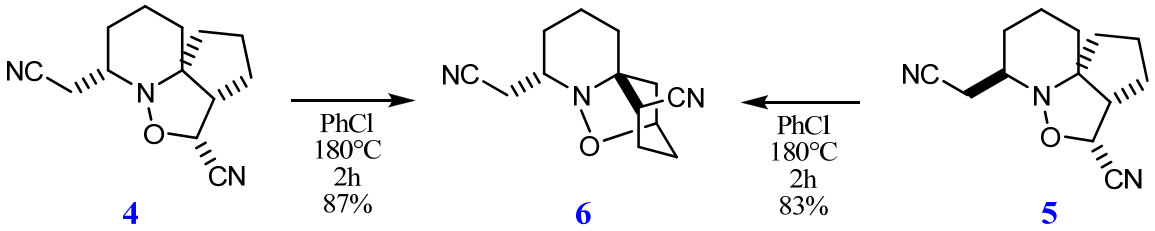

Figure 5.4. Conversion of the 6,5,5 tricycles *4* and *5* to the 6,6,5 isomer *6*.

5.3.1. Conformational Study

5.3.1.1. Conformational Analysis of the Reactants and Products. Conformational analysis showed that the 6,6,5-tricyclic adduct *6* (Figure 5.5d) has the lowest energy among the all products and the reactant; nitrone, *3* (Figure 5.5a). It is more stable than the nitrone by 15.5 kcal/mol in terms of Gibbs free energy (B3LYP/6-31+G(d)//M06-2X/6-311+G(d,p)). The tricyclic adducts *4*, *5* and *6* have lower energies than nitrone. The 6,5,5-adduct *5* (Figure 5.5c) is preferred over its diastereomer *4* (Figure 5.5b) by 3.3 kcal/mol.

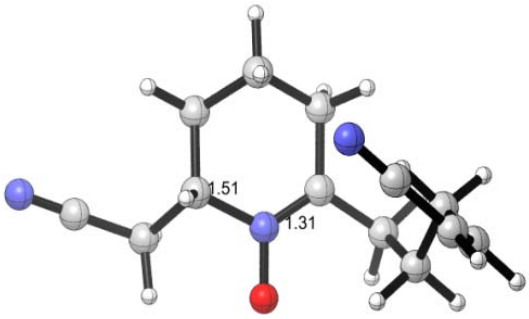

(a) *3* (15.5 kcal/mol)

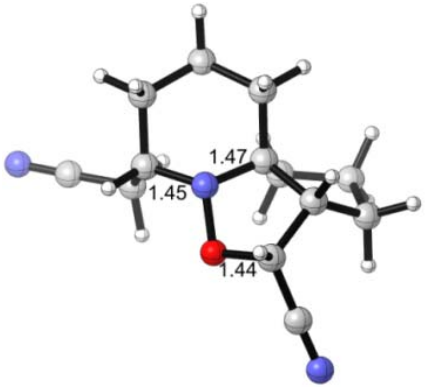

(b) *4* (8.5 kcal/mol)

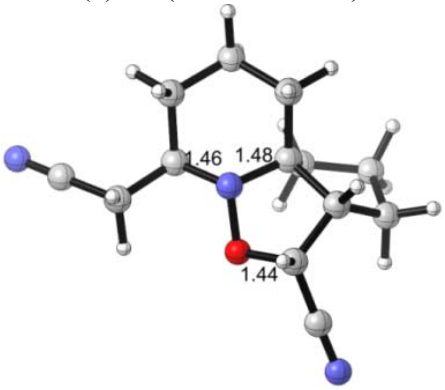

(c) *5* (5.2 kcal/mol)

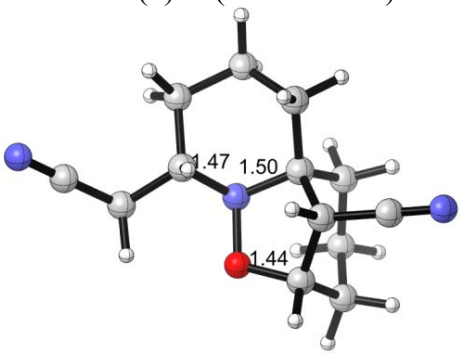

(d) *6* (0.0 kcal/mol)

Figure 5.5. Conformational analysis of nitrone and tricyclic products.

5.3.1.2. Conformational Analysis of Transition States. The transition state structures in the path of interconversion of *3* to *4*, *5* and *6* are investigated by taking into account the possible pathways of the reaction. Holmes et. al proposed a cyclic mechanism (Figure 5.6) for the interconversion of 6,6,5- and 6,5,5-tricycles.

In the cyclic mechanism (Figure 5.6), the interconversion of all species to *6* is shown. At elevated temperature the conversion of *3* to *6* is possible. Because *3* has two enantiomers, as a result *6* will be obtained in two different diastereomers which is not useful in organic synthesis. In order to make it possible to obtain just one diastereomer of *6*, the cyclic mechanism is proposed. In this pathway besides the interconversion of species to *6*, there is also the conversion of *4* to *5* and vice versa via nitrile compound, *8*.

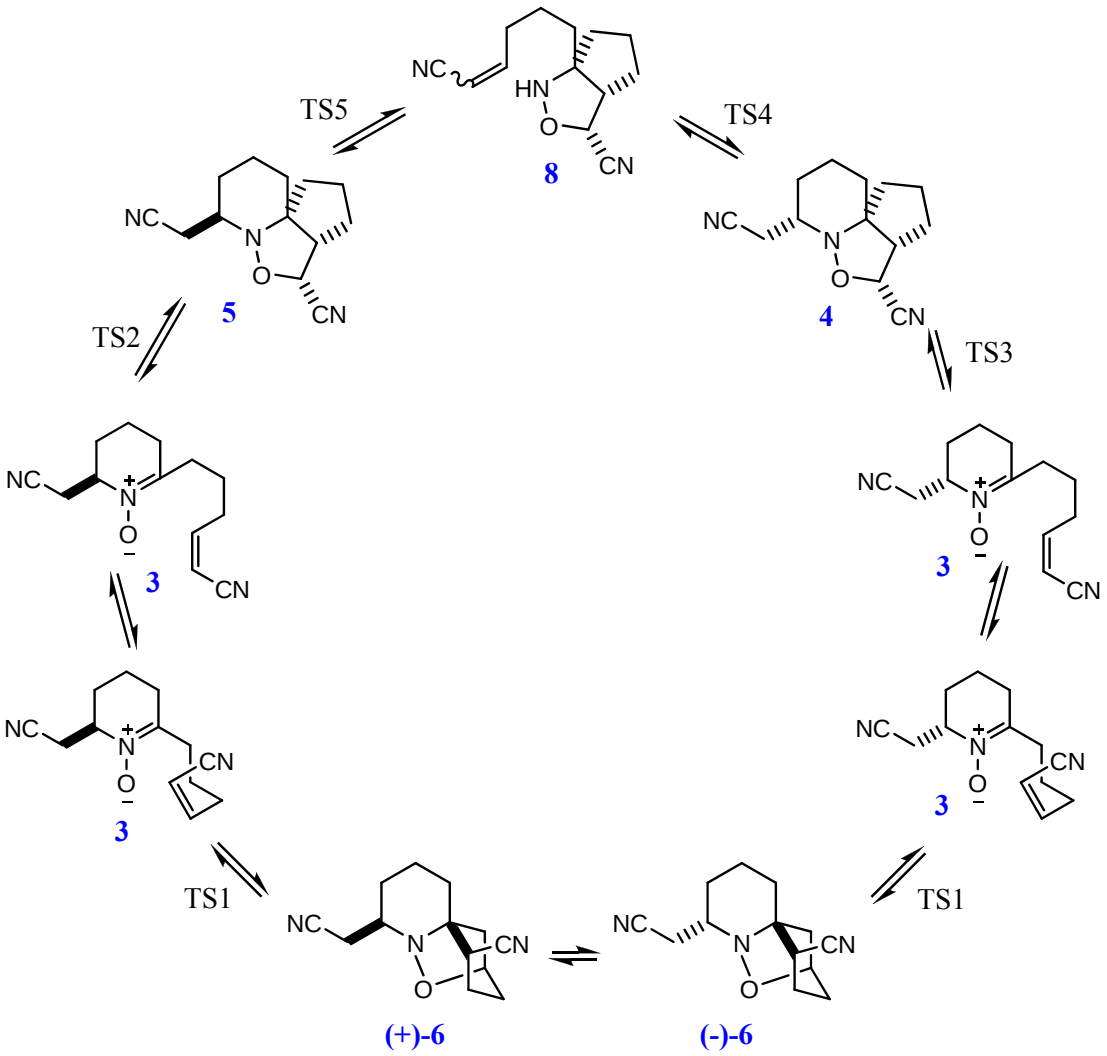

Figure 5.6. Possible mechanism for the interconversion of 6,6,5- and 6,5,5- tricycles.

Density functional calculations were done and the best transition state structures were found. The structures and the energies relative to the *6*, which is the reactant with lowest energy are reported in Figure 5.7. The lowest transition state in terms of M06-2X single point energies belongs to the conversion of *3* to *6*, *TS1*. Therefore the *TS1* is the easiest transition state, the cyclic mechanism for the interconversion of *4* and *5* should be achieved.

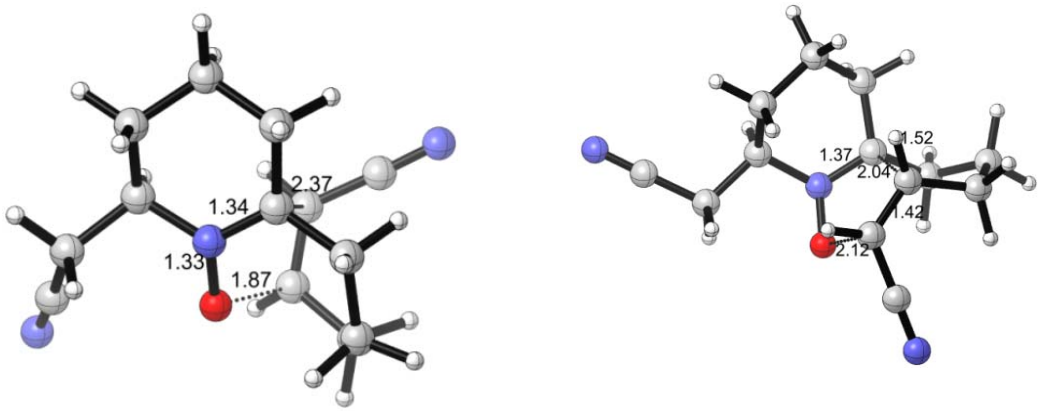

TS1
31.1
(38.7)

TS2
31.6
(41.7)

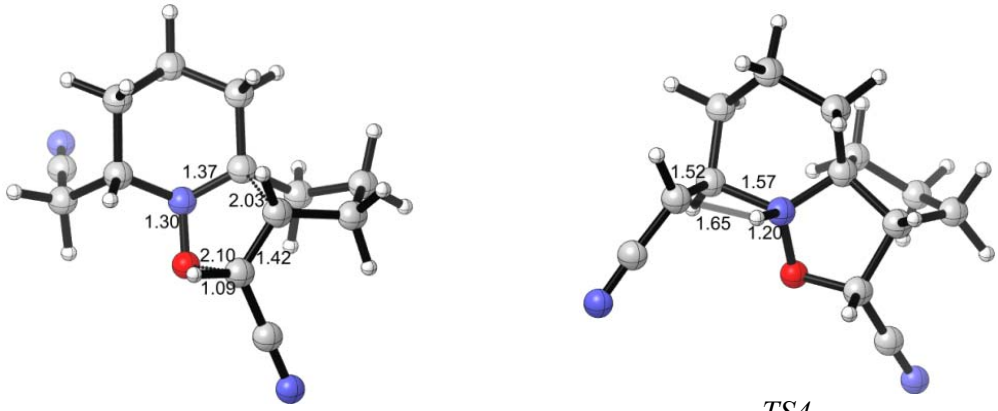

TS3
30.5
(40.6)

TS4
65.3
(65.9)

Figure 5.7. Transition state structures and Gibbs free energies (B3LYP/6-31+G(d)). M06-2X/6-311+G(d,p) single point energies are given in parenthesis.

The transition state energies of *4*, *5* and *6* are close to each other and thus render the interconversion possible. But the energy of *TS4* is very high compared to others. Because of this high energy it was hard to locate it, whereas *TS5* cannot be located and energy

could not be obtained. High energy barriers of *TS4* to get *6*, make the cyclic mechanism difficult and maybe even not possible.

5.3.2. Reaction Mechanism

In the interconversion of the species into *6* there should be another pathway with lower energy than via-nitrile mechanism. Because *4* and *5* are also diastereomers that both formed via *3*, the new pathway should include enantiomerization of *3*. As shown in Figure 5.3, *3* is generated from an achiral oxime (*2*) in two diastereomers to give *4*, *5* and *6*. Because of the high energy during *TS4* and *TS5* (Figure 5.8 (a)), an alternative mechanism is proposed via enantiomerization of *3* (Figure 5.8 (b)).

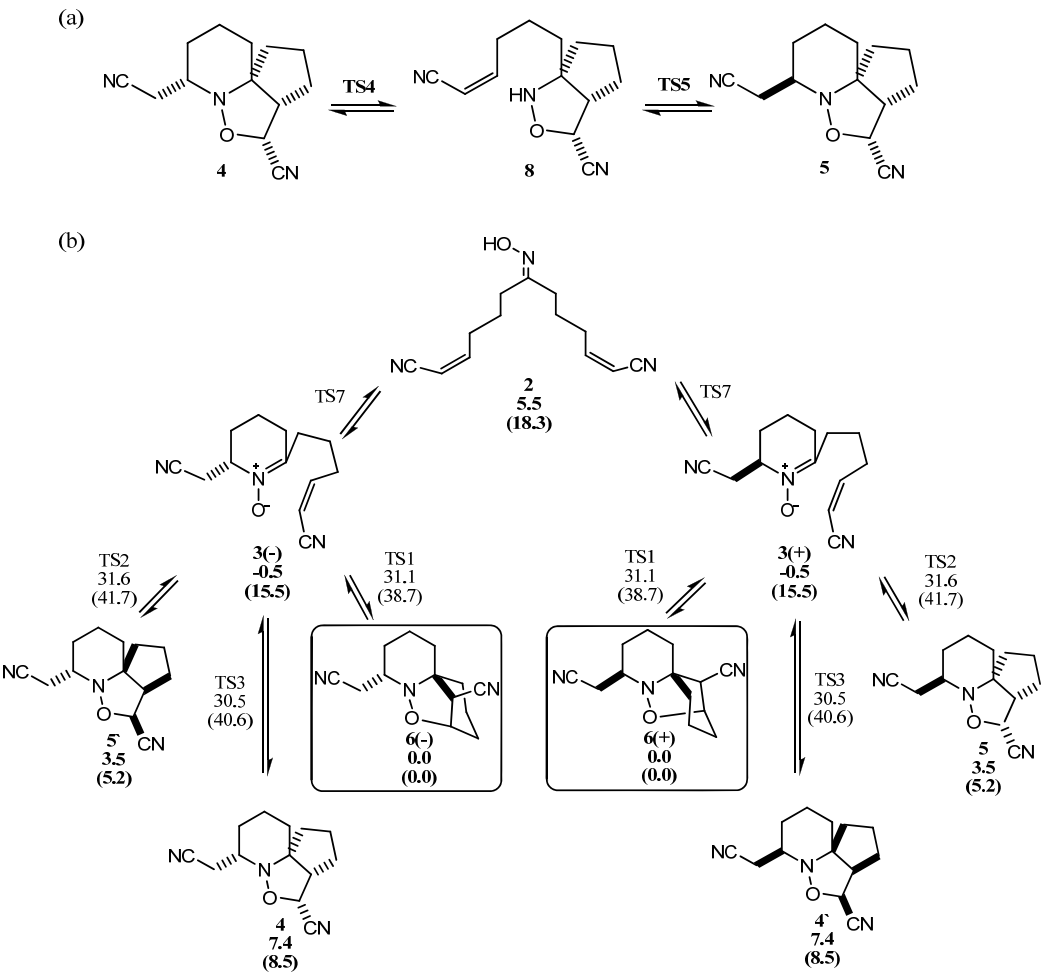

Figure 5.8. (a) interconversion via-nitrile (b)interconversion via-oxime mechanisms. Gibbs free energies (B3LYP/6-31+G(d) and B3LYP/6-31+G(d)//M06-2X/6-311+G(d,p) in parentheses) are given.

Alternative mechanism involves the epimerization of *3* via oxime compound (Figure 5.9). The 6,6,5-tricycle *6* has the lowest energy and the tabulated energies are given relative to that. The oxime is generated by an achiral ketone and it is achiral also. Because of being achiral it produces *4*, *5* and *6* with their mirror images, *4(+)*, *4(-)*, *5(+)*, *5(-)*, *6(+)* and *6(-)*. *TS7* is shown in Figure 5.9. It has energy of 29.7 kcal/mol relative to *6* in terms of B3LYP/6-31+G(d) energies which indicates that the alternative mechanism is energetically preferred to cyclic mechanism.

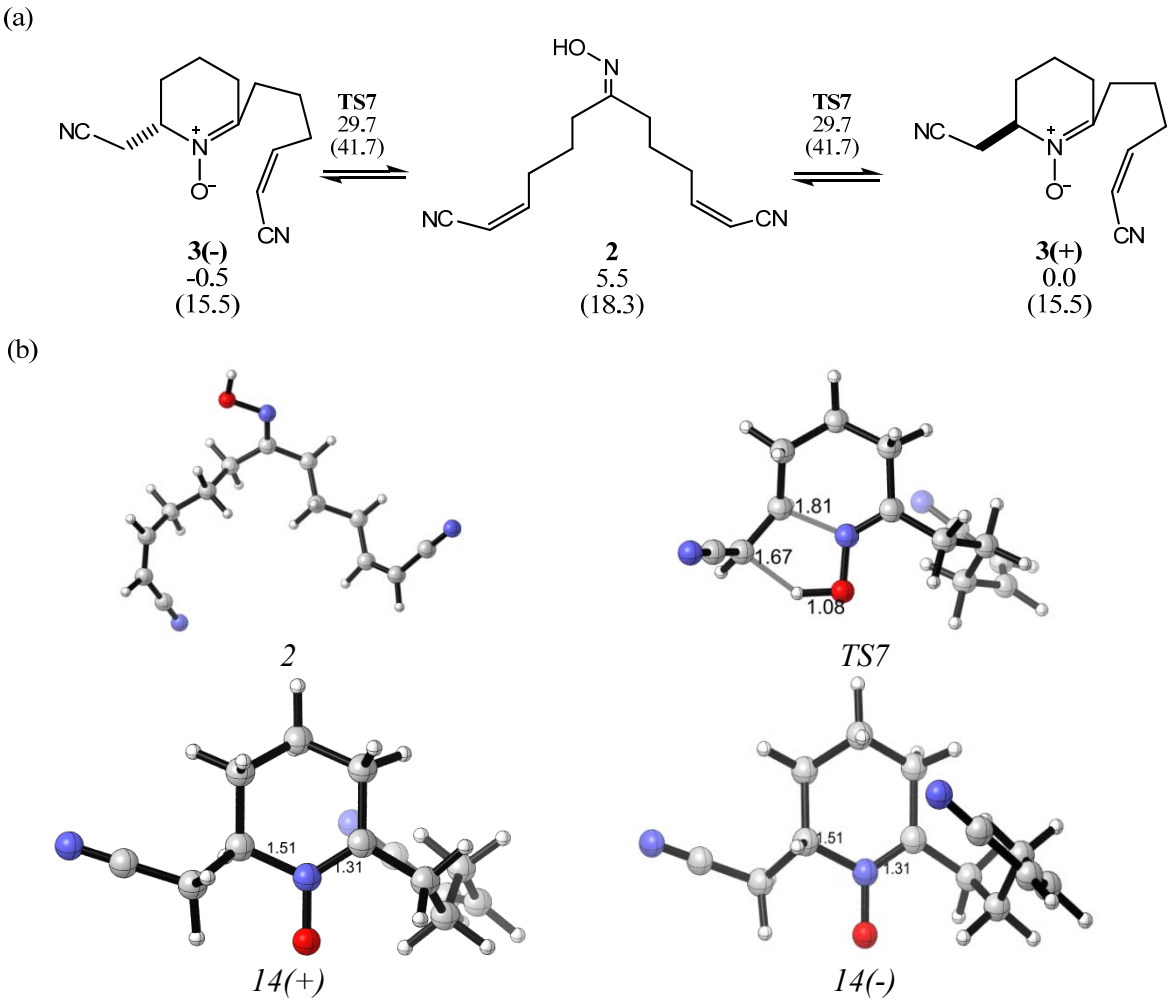

Figure 5.9. (a) Epimerization of *3*. Gibbs free energies (B3LYP/6-31+G(d) and B3LYP/6-31+G(d)/M06-2X/6-311+G(d,p) in parentheses) are given. (b) Reactants and transition state structure of enantiomerization pathway.

Both B3LYP and M06-2X predict the 6,6,5 tricycle *6* to be the thermodynamic product from cycloaddition of *3*, consistent with experiment [83]. B3LYP calculations

indicate that the 6,5,5 tricycles *4* and *5* lie 7.4 and 3.5 kcal/mol above *6*, respectively. Similar relative energies for the three species are provided by the M06-2X single-point calculations (*4*, *5*, and *6* = 8.5, 5.2, and 0 kcal/mol, respectively). The equatorial isomer *5* in the 6,5,5 series is 3 kcal/mol more stable than the axial isomer *4*.

It has been found that 6,6,5-tricyclic nitrone products are more stable than the 6,5,5-tricyclic ones. The trend is same in case of hydrocarbons 6,6,5-tricyclic one, *H6,5,5* is 0.05 kcal/mol more stable than *H6,6,5* (Figure 5.10).

H6,5,5
0.05

H6,6,5
0.0

Figure 5.10. Relative energies of 6,5,5 and 6,6,5- tricyclic hydrocarbons.

In order to investigate why the energy gap gets larger, several computations are conducted. First, the nitrone (N-O) effect is sought. All the –CN substituents are removed and the computations are done. The same trend is observed as in previous findings (Figure 5.11).

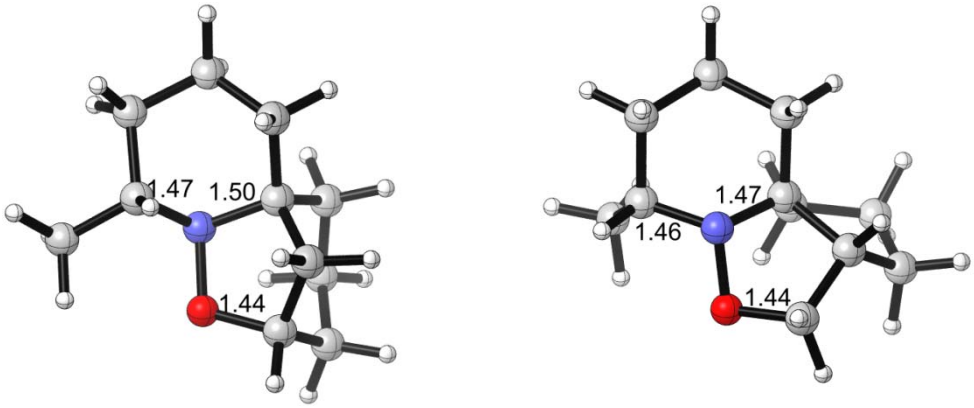

6H
0.0

4H
5.3

Figure 5.11. Relative energies of *5* and *6* without CN (kcal/mol).

It has been seen that nitrone (N-O) has a role on favoring [6,6,5] more by 5.3 kcal/mol energy difference. The same investigation is conducted for –CN substituent effect and in these calculations nitrone effect is taken away by conversion of nitrogen and oxygen heteroatoms to carbon atoms. The resultant tricycles are shown in Figure 5.12 with their relative energies.

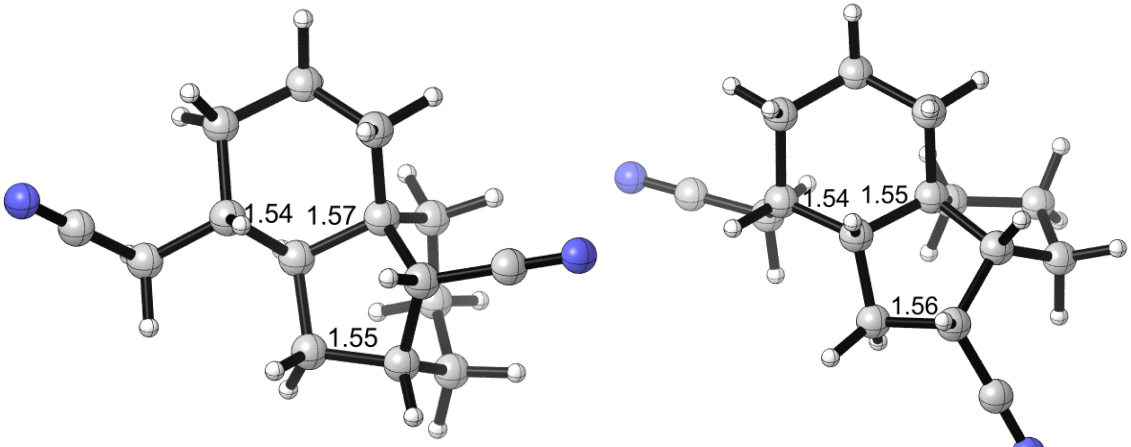

HC6,6,5
0.0

HC6,5,5
5.1

Figure 5.12. Relative energies of *5* and *6* without nitrone component (N-O) (kcal/mol).

HC6,6,5, *6* without nitrone character is more stable than *HC6,5,5* one by 5.1 kcal/mol. As a result, the favorable [6,5,5] becomes more unstable in case of both –CN substituent and nitrone character. In both cases *6* derivatives are energetically favorable with approximately 5 kcal/mol energy.

In previous studies, the same intramolecular nitrone cycloaddition is done experimentally by using different substituents instead of –CN group, for example, R=H [96-97], Bu [97] or COOMe [96]. As a first study on substituent effect in nitrone cycloaddition, reaction has been modeled with no substituent, R=H (Figure 5.13).

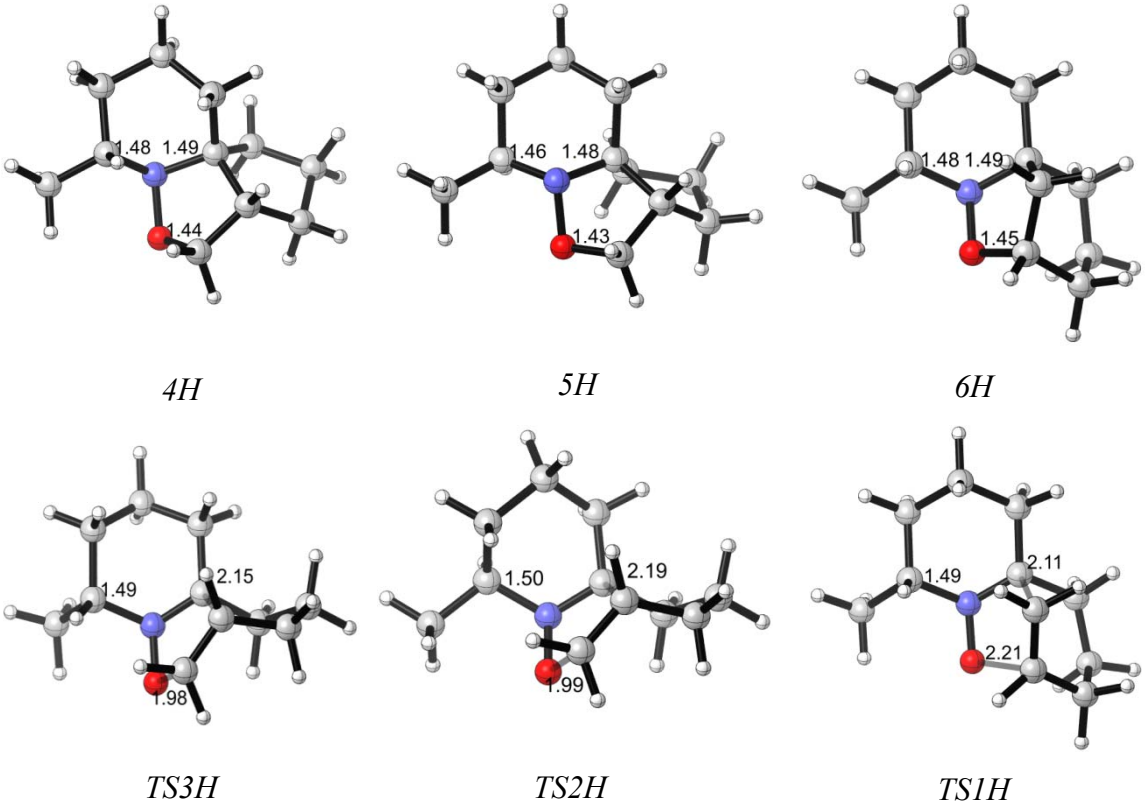

Figure 5.13. Reactants and transition state structures in case of R=H.

The energies of the cycloaddition reaction with R=H are tabulated in Table 5.1 and compared with the energies of R=CN in parentheses.

Table 5.1. Gibbs free energies of the reactants and transition states of the reaction R=H and R=CN (B3LYP/6-31+G(d)).

R=H (R=CN)	***15***	***16***	***17***	***TS1***	***TS2***	***TS3***
rel E	5.3 (7.7)	0.0 (0.0)	4.0 (3.9)	39.3 (33.7)	40.6 (34.4)	39.6 (33.7)
rel H	5.4 (7.5)	0.0 (0.0)	4.1 (3.7)	37.3 (31.8)	38.7 (32.5)	37.8 (31.9)
rel G	4.6 (7.9)	0.0 (0.5)	3.6 (4.0)	36.2 (31.6)	37.5 (32.1)	36.3 (31.0)

The trend between the relative energies does not change as R changes from –CN to –H that can be seen from Table 5.1. The 6,6,5-tricycle is the most stable product of the reaction.

5.4. Conclusions and Future Work

The intramolecular nitrone 1,3-dipolar cycloaddition is modeled and its regioselectivity and stereoselectivity are investigated. In the reaction, two types of tricycles are produced; one is 6,5,5-tricycle with its diastereomer and 6,6,5-tricycle which is the core intermediate for the synthesis of histrionicotoxins. The aim is to convert 6,5,5-tricycles to 6,6,5- in high selectivity.

First, the already proposed mechanism is modeled and high energies are found for the interconversion of *6(+)* to *6(-)*. Then, an alternative pathway is generated and an energetically favorable pathway is proposed. The alternative mechanism involves the enantiomerization of nitrone compound *3* which gives lower energy barriers. As a result the interconversion of 6,5,5-tricyclic products to the desired 6,6,5-tricyclic one is achieved with the new mechanism.

From previous studies it is understood that the substituent on the nitrone has an important role on the regioselectivity and stereoselectivity. So that, a reaction is modeled with R=H instead of R=CN. But again 6,6,5- found to be most stable product instead of 6,5,5- as claimed in experimental case.

For the further understanding the substituent effect on selectivity of the nitrone cycloaddition reaction, the effect of different substituents will be investigated. Also the effect of the solvent will be modeled and compared with the experimental data.

REFERENCES

1. Woodward, R. B. and R. Hoffmann, *The Conservation of Orbital Symmetry*, Academic Press, New York, 1970.

2. Fleming, I., *Pericyclic Reactions*, Oxford University Press, New York, 1999.

3. Carey, F. A. and R. J. Sundberg, *Advanced Organic Chemistry,* Springer, Virginia, 2008.

4. Kobayashi, S. and K. A. Jørgensen, *Cycloaddition Reactions in Organic Synthesis*, Wiley-WCH, Germany, 2002.

5. Houk, K. N., Y.-T. Lin and F. K. Brown, "Evidence for the Concerted Mechanism of the Diels-Alder Reaction of Butadiene with Ethylene", *J. Am. Chem. Soc.*, Vol. 108, pp. 554-556, 1986.

6. Kobuke, Y., T. Sugimoto, J. Furukawa and T. Funco, "Role of Attractive Interactions in Endo-Exo Stereoselectivities of Diels-Alder Reactions", *J. Am. Chem. Soc.*, Vol. 94, pp. 3633-3365, 1972.

7. Williamson, K. L. and Y.-F. L. Hsu, "Stereochemistry of Diels-Alder Reaction. II. Lewis Acid Catalysis of Syn-Anti Isomerism", *J. Am. Chem. Soc.*, Vol. 92, pp. 7385-7389, 1970.

8. Dewar, M. J. S. and A. B. Pierini, "Mechanism of the Diels-Alder Reaction - Studies of the Addition of Maleic-Anhydride to Furan and Methylfurans", *J. Am. Chem. Soc.*, Vol. 106, pp. 203-208, 1984.

9. Carruthers, W., *Cycloaddition Reactions in Organic Synthesis*, Pergamon Press, New York, 1990.

10. Boger, D. L. and S. M. Weinreb, *Hetero Diels-Alder Methodology in Organic Synthesis*, Academic Press, San Diego, 1987.

11. Coxon, J. M., *Advances in Detailed Reaction Mechanisms*, Vol. 3, JAI Press, Greenwich, 1994.

12. Houk, K. N., J. Gonzales and Y. Li, "Pericyclic Reaction Transition States – Passions and Punctilios, 1935-1995", *Acc. Chem. Res.*, Vol. 28, pp. 81-90, 1995.

13. Nicolaou, K. C., S. A. Snyder, T. Montagnon and G. Vassilikogiannakis, "The Diels-Alder Reaction in Total Synthesis", *Angew. Chem. Int. Ed.*, Vol. 41, pp. 1668-1698, 2002.

14. Corey, E. J., "Catalytic Enantioselective Diels-Alder Reactions: Methods, Mechanistic Fundamentals, Pathways and Applications", *Angew. Chem. Int. Ed.*, Vol. 41, pp. 1650-1667, 2002.

15. Castro, A. M. M., "Claisen Rearrangement Over the Past Nine Decades", *Chem. Rev.*, Vol. 104, pp. 2939–3002, 2004.

16. Hiersemann, M. and U. Nubbemeyer, *The Claisen Rearrangement*, Wiley-VCH, 2007.

17. Nubbemeyer, U., "Recent Advances in Asymmetric [3,3]-Sigmatropic Rearrangements", *Synthesis*, Vol. 7, pp. 961-1008, 2003.

18. Breuer, E., H. G. Aurich, A. Nielsen, *Nitrones, Nitronates and Nitroxides*, John Wiley and Sons: Chichester, pp. 139-312, 1989.

19. Tuffariello, J. J., 1*,3-Dipolar Cycloaddition Chemistry*, John Wiley and Sons: New York, Vol. 2, pp. 83-168, 1984.

20. Black, D. St. C., R. F. Crozier, and V. C. Davis, "1,3-Dipolar Cycloaddition Reactions of Nitrones", *Synthesis*, pp. 205-211, 1975.

21. Becke, A. D., "Density-Functional Exchange Energy Approximation with Correct Asymptotic Behavior", *Phys. Rev. A*., Vol. 38, pp. 3098-3103, 1988.

22. Becke A. D., "A New Mixing of Hartree-Fock and Local Density Functional Theories", *J. Chem. Phys*., Vol. 38, pp. 1372-1377, 1993.

23. Parr, R. G. and W. Yang, *Density Functional Theory of Atoms and Molecules*, Oxford University Press, New York, 1989.

24. Handy, N. C., "Density Functional Theory", in: B. O. Roos (ed.), Lecture Notes in Quantum Chemistry, Vol. 2, pp. 91-123, Springer-Verlag, Berlin, 1994.

25. Leach, A. R., *Molecular Modelling Principles and Applications*, Prentice Hall, England, 2001.

26. Lee, C., W. Yang and R. G. Parr, "Development of Colle-Salvatti Correlation Energy Formula into a Functional of the Electron Density", *Phys. Rev. B*, Vol. 37, pp. 785-789, 1988.

27. Becke, A. D., "Density Functional Thermochemistry. III. The Role of Exact Exchange", *J. Chem. Phys*., Vol. 98, pp. 5648-5652, 1993.

28. Pauling, L. J., "The Nature of the Chemical Bond. IV. The Energy of Single Bonds and the Relative Electronegativity of Atoms", *J. Am. Chem. Soc*., Vol. 54, pp. 3570-3582, 1932.

29. Tapia, O. and J. *Bertrán,* Solvent Effects and Chemical Reactivity*,* Kluwer Academic Publishers, The Netherlands, 1996.

30. Cramer, C. J. and D. G. Truhlar, "Implicit Solvation Models: Equilibria, Structure, Spectra, and Dynamics", *Chem. Rev.*, Vol. 99, pp. 2162-220, 1999.

31. Tomasi, J., B. Mennucci and R. Cammi, "Quantum Mechanical Continuum Solvation Models", *Chem. Rev.*, Vol. 105, pp. 2999-3093, 2005.

32. Barone, V., M. Cossi and J. Tomasi, "Geometry Optimization of Molecular Structures in Solution by the Polarizable Continuum Model", *J. Comp. Chem.*, Vol.19, pp. 404-417, 1998.

33. Barone, V. and M. Cossi, "Quantum Calculation of Molecular Energies and Energy Gradients in Solution by a Conductor Solvent Model", *J. Phys. Chem. A*, Vol. 102, pp. 1995-2001, 1998.

34. Kozmin, S. A. and V. H. Rawal, "Chiral Amino Siloxy Dienes in the Diels-Alder Reaction: Applications to the Asymmetric Synthesis of 4-Substituted and 4,5-Disubstituted Cyclohexenones and the Total Synthesis of (-)-Alpha-Elemene", *J. Am. Chem. Soc.*, Vol. 121, pp. 9562–9573, 1999.

35. Janey, J. M., T. Iwama, S. A. Kozmin and V. H. Rawal, "Racemic and Asymmetric Diels-Alder Reactions of 1-(2-oxazolidinon-3-yl)-3-siloxy-1,3-butadienes", *J. Org. Chem*., Vol. 65, pp. 9059–9068, 2000.

36. Çelebi-Ölçüm, N., A. Sanyal and V. Aviyente, "Understanding the Stereoselection Induced by Chiral Anthracene Templates in Diels-Alder Cycloaddition: A DFT Study", *J. Org. Chem*., Vol. 74, pp. 2328-2336, 2009.

37. Sanyal, A. and J. K. Snyder, "Stereoselective Diels-Alder Reactions of Chiral Anthracenes", *Org. Lett.*, Vol. 2, pp. 2527–2530, 2000.

38. Corbett, M. S., X. Liu, A. Sanyal and J. K. Snyder, "Cycloadditions of Chiral Anthracenes: Effect of the Trifluoromethyl Group", *Tetrahedron Lett*., Vol. 44, pp. 931–935, 2003.

39. Burgess, K. L., M. S. Corbett, P. Eugenio, N. J. Lajkiewicz, X. Liu, A. Sanyal, W. Yan, Q. Yuan, J. K. Snyder, "Chiral Anthracene and Anthrone Templates as Stereocontrolling Elements in Diels-Alder/retro Diels-Alder Sequences", *Bioorg. Med. Chem.*, Vol. 13, pp. 5299–5309, 2005.

40. Sanyal, A., Q. Yuan, J. K. Snyder, "A New, Chiral Aminoanthracene for the Diels-Alder/Retro-Diels-Alder Sequence in Lactam and Butenolide Synthesis", *Tetrahedron Lett.*, Vol. 46, pp. 2475–2478, 2005.

41. Burgess, K. L., N. J. Lajkiewicz, A. Sanyal, W. Yan and J. K. Snyder, "A New Chiral Anthracene for the Asvmmetric Diels-Alder/retro-Diels-Alder Sequence", *Org. Lett.*, Vol. 7, pp. 31-34, 2005.

42. Jones, A. L., X. Liu and J. K. Snyder, "Enantioselective Syntheses of Candenatenins B and C Using a Chiral Anthracene Auxiliary", *Tetrahedron Lett.*, Vol. 51, pp. 1091-1094, 2010.

43. Jones, S. and J. C. C. Atherton, "Highly Diastereoselective Photochemical Diels-Alder Reactions: Towards the Development of a Photoactivated Chiral Auxiliary", *Tetrahedron: Asymmetry*, Vol. 12, pp. 1117–1119, 2001.

44. Atherton, J. C. C. and S. Jones, "Diastereomeric Control of Photoinduced Diels-Alder Reactions of 1-anthracen-9-yl-Ethanol by Hydrogen-Bonding Effects", *Tetrahedron Lett.*, Vol. 42, pp. 8239–8241, 2001.

45. Atherton, J. C. C. and S. Jones, "Establishing Cleavage Conditions for an Anthracene Chiral Auxiliary Using a Photochemical Retro Diels-Alder Reaction" *Tetrahedron Lett.*, Vol. 43, pp. 9097–9100, 2002.

46. Atherton, J. C. C. and S. Jones, "Mechanistic Investigations in Diastereoselective Diels-Alder Additions of Chiral 9-anthrylethanol Derivatives", *J. Chem. Soc., Perkin Trans. 1*, pp. 2166–2173, 2002.

47. Bawa, R. A. and S. Jones, “Synthesis and Diels-Alder Reactions of 9-(4-benzyloxazolin-2-yl) Anthracene”, *Tetrahedron*, Vol. 60, pp. 2765–2770, 2004.

48. Ess, D. H. and K. N. Houk, “Distortion/Interaction Energy Control of 1,3-dipolar Cycloaddition Reactivity”, *J. Am. Chem. Soc.*, Vol. 129, pp. 10646-10647, 2007.

49. Schoenebeck, F., D. H. Ess, G. O. Jones and K. N. Houk, “Reactivity and Regioselectivity in 1,3-Dipolar Cycloadditions of Azides to Strained Alkynes and Alkenes: A Computational Study”, *J. Am. Chem. Soc.*, Vol. 131, pp. 8121-8133, 2009.

50. Catak, S., M. D’hooghe, N. De Kimpe, M. Waroquier and V. Van Speybroeck, “Intramolecular pi-pi Stacking Interactions in 2-Substituted N,N-Dibenzylaziridinium Ions and Their Regioselectivity in Nucleophilic Ring-Opening Reactions”, *J. Org. Chem.*, Vol. 75, pp. 885-896, 2010.

51. Ess, D. H. and K. N. Houk, “Theory of 1,3-dipolar Cycloadditions: Distortion/Interaction and Frontier Molecular Orbital Models”, *J. Am. Chem. Soc.*, Vol. 130, pp. 10187-10198, 2008.

52. de Jong, G. T. and F. M. Bickelhaupt, “ Transition-State Energy and Position Along the Reaction Coordinate in an Extended Activation Strain Model”, *ChemPhysChem*, Vol. 8, pp. 1170-1181, 2007.

53. van Eis, M. J., F. M. Bickelhaupt, S. van Loon, M. Lutz, A. L. Spek, W. H. de Wolf, W. J. van Zeist and F. Bickelhaupt, “Tricarbonylchromium Complexes of [5]- and [6]metacyclophane: an Experimental and Theoretical Study”, *Tetrahedron*, Vol. 64, pp. 11641–11646, 2008.

54. van Zeist, W. J. and F. M. Bickelhaupt, “The Activation Strain Model of Chemical Reactivity”, *Org. Biomol. Chem.,* Vol. 8, pp. 3118-3127, 2010.

55. Domingo, L. R., M. J. Aurell, M. Arnó and J. A. Sáez, "Toward an Understanding of the Acceleration of Diels-Alder Reactions by a Pseudo-Intramolecular Process Achieved by Molecular Recognition. A DFT Study", *J. Org. Chem.*, Vol. 72, pp. 4220-4227, 2007.

56. Padwa, A., K. R. Crawford, C. S. Straub, S. N. Pieniazek and K. N. Houk, "Halo Substituent Effects on Intramolecular Cycloadditions Involving Furanyl Amides", *J. Org. Chem.*, Vol. 71, pp. 5432-5439, 2006.

57. Pieniazek, S. N. and K. N. Houk, "The Origin of the Halogen Effect on Reactivity and Reversibility of Diels-Alder Cycloadditions Involving Furan", *Angew. Chem. Int. Ed.*, Vol. 45, pp. 1442 –1445, 2006.

58. Frisch, M. J., et al. *Gaussian 03*, revision D.01; Gaussian, Inc.: Wallingford CT, 2004.

59. Boese, A. D. and J. M. L. Martin, "Development of Density Functionals for Thermochemical Kinetics", *J. Chem. Phys.*, Vol. 121, pp. 3405–3416, 2004.

60. Hajduch, J., O. Paleta, J. Kvíčala and G. Haufe, "Fluorinated Furan-2(5H)-ones: Reactivity and Stereoselectivity in Diels-Alder Reactions", *Eur. J. Org. Chem.*, pp. 5101–5111, 2007.

61. Dkhissi, A. and R. Blossey, "Performance of DFT/MPWB1K for Stacking and H-Bonding Interactions", *Chemical Physics Letters*, Vol. 439, pp. 35–39, 2007.

62. Wheeler, S. E., A. Moran, S. N. Pieniazek and K. N. Houk, "Accurate Reaction Enthalpies and Sources of Error in DFT Thermochemistry for Aldol, Mannich, and alpha-Aminoxylation Reactions", *J. Phys. Chem. A*, Vol. 113, pp. 10376–10384, 2009.

63. Pieniazek, S. N., F. R. Clemente and K. N. Houk, "Sources of Error in DFT Computations of C-C Bond Formation Thermochemistries: Pi->Sigma Transformations and Error Cancellation by DFT Methods", *Angew. Chem. Int. Ed.*, Vol. 47, pp. 7746 –7749, 2008.

64. Frisch, M. J., et al. Gaussian 09, revision A.1; Gaussian, Inc.: Wallingford CT, 2009.

65. Gonzalez, C. and H. B. Schlegel, "An Improved Algorithm for Reaction-Path Following", *J. Chem. Phys.*, Vol. 90, pp. 2154-2161, 1989.

66. Gonzalez, C. and H. B. Schlegel, "Reaction Path Following in Mass Weighted Internal Coordinates", *J. Phys. Chem.*, Vol. 94, pp. 5523-5527, 2000.

67. Mennucci, B. and J. Tomasi, "Continuum Solvation Models: A New Approach to the Problem of Solute's Charge Distribution and Cavity Boundaries", *J. Chem. Phys.*, Vol. 106, pp. 5151-5158, 1997.

68. Mennucci, B., E. Cancès and J. Tomasi, "Evaluation of Solvent Effects in Isotropic and Anisotropic Dielectrics and in Ionic Solutions with a Unified Integral Equation Method: Theoretical Bases, Computational Implementation, and Numerical Applications", *J. Phys. Chem. B.*, Vol. 101, pp. 10506-10517, 1997.

69. Thompson, J. D., C. J. Cramer and D. G. Truhlar, "Predicting Aqueous Solubilities from Aqueous Free Energies of Solvation and Experimental or Calculated Vapor Pressures of Pure Substances", *J. Chem. Phys*., Vol. 119, pp. 1661-1670, 2003.

70. Kelly, C. P., C. J. Cramer and D. G. Truhlar, "SM6: A Density Functional Theory Continuum Solvation Model for Calculating Aqueous Solvation Free Energies of Neutrals, Ions, and Solute-Water Clusters", *J. Chem. Theory Comput*., Vol. 1, 1133-1152, 2005.

71. van Eis, M. J. and F. M. Bickelhaupt, “Tricarbonylchromium Complexes of [5]- and [6]metacyclophane: An Experimental and Theoretical Study”, *Tetrahedron,* Vol. 64, pp. 11641–11646, 2008.

72. Tripathy, R., R. W. Franck and K. D. Onan, “Diels-Alder Reaction of Dienes Having Stereogenic Allylic Substituents - Control of Diastereoface Selectivity by the Dienophile”, *J. Am. Chem. Soc.*, Vol. 110, pp. 3257-3262, 1988.

73. Adam, W., J Gläser., K. Peters and M. Prein, “Highly Like-Selective [4+2]-Cycloadditions of Chiral Dienols - The Importance of 1,3-Allylic Strain in the Hydroxy-Directed Stereocontrol”, *J. Am. Chem. Soc.*, Vol. 117*,* pp. 9190-9193, 1995.

74. Salem, L., “Intermolecular Orbital Theory of Interaction Between Conjugated Systems .2. Thermal and Photochemical Cycloadditions”, *J. Am. Chem. Soc.*, Vol. 90, pp. 553-566, 1968.

75. Alston, P. V., R. M. Ottenbrite and T. Cohen, “Secondary Orbital Interactions Determining Regioselectivity in Diels-Alder Reaction .3. Disubstituted Dienes”, *J. Org. Chem.*, Vol. 43, pp. 1864-1867, 1978.

76. Ginsburg, D., “The Role of Secondary Orbital Interactions in Control of Organic-Reactions”, *Tetrahedron*, Vol. 39, pp. 2095-2135, 1983.

77. Gleiter, R. and M. C. Böhm, “Regioselectivity and Stereoselectivity in Diels-Alder Reactions - Theoretical Considerations”, *Pure Appl.Chem.*, Vol. 55, pp. 237-244, 1983.

78. Birney, D. M. and K. N. Houk, “Transition Structures of the Lewis Acid-Catalyzed Diels-Alder Reaction of Butadiene with Acrolein - The Origins of Selectivity” *J. Am. Chem. Soc.*, Vol. 112, pp. 4127-4133, 1990.

79. Singleton, D. A., "A [4 + 3] Transition-State for a [4 + 2] Cycloaddition - A New Secondary Orbital Interaction in Diels-Alder Reactions", *J. Am. Chem. Soc.*, Vol. 114, pp. 6563-6564, 1992.

80. Ohwada, T., "Orbital-Controlled Stereoselections in Sterically Unbiased Cyclic Systems", *Chem. Rev.*, Vol. 99, pp. 1337-1375, 1999.

81. Arrieta, A., F. P. Cossío, B. Lecea, "Direct Evaluation of Secondary Orbital Interactions in the Diels-Alder Reaction Between Cyclopentadiene and Maleic Anhydride", *J. Org. Chem.*, Vol. 66, pp. 6178-6180, 2001.

82. Wannere, C. S., A. Paul, R. Herges, K. N. Houk, H. F. Schaefer III and P. v. R. Schleyer, "The Existence of Secondary Orbital Interactions", *J. Comput. Chem.*, Vol. 28, pp. 344-361, 2007.

83. Horsley, H. T., A. B. Holmes, J. E. Davies, J. M. Goodman, M. A. Silva, S. I. Pascu and I. Collins, "Nitrone Dipolar Cycloaddition Routes to Piperidines and Indolizidines Part 10 - Investigation of Conjugate Addition/Intramolecular Nitrone Dipolar Cycloadditions and Their Use in the Synthesis of Dendrobatid Alkaloid Precursors", *Org. Biomol. Chem.*, Vol. 2, pp. 1258 – 1265, 2004.

84. Beckmann, E., "Zur Kenntniss der Aldoxime. VII", *Ber. Dtsch. Chem. Ger.*, Vol. 23, pp. 3331-3341, 1890.

85. Beckmann, E., "Ueber die Reaction Zwischen N-Aldoximäthern und Phenylisocyanat", *Ber. Dtsch. Chem. Ger.*, Vol. 27, pp. 1957-1959, 1894.

86. Pfeiffer, P., "Lichtchemische Synthese von Indolderivaten", *Annalen*, Vol. 411, pp. 72-158, 1916.

87. Padwa, A. and W. H. Pearson, *Synthetic Applications of 1,3-Dipolar Cycloaddition Chemistry Toward Heterocycles and Natural Products,* John Wiley & Sons, Inc., New Jersey, 2003.

88. Huisgen, R., “Kinetics and Mechanism of 1,3-Dipolar Cycloadditions”, *Angewandte Chemie International Edition*, Vol. 2, pp. 633–645, 1963.

89. Huisgen, R., “1,3-Dipolar Cycloadditions. Past and Future”, *Angewandte Chemie International Edition*, Vol. 2, pp. 565–598, 1963.

90. Williams, G. M., S. D. Roughley, J. E. Davies, A. B. Holmes and J. P. Adams, “Synthesis of (-)-Histrionicotoxin by a Tandem Process”, *J. Am. Chem. Soc.*, Vol. 121, pp. 4900–4901, 1999.

91. Smith, C. J., A. B. Holmes and N. J. Press, “The Total Synthesis of Alkaloids (-)-Histrionicotoxin 259A, 285C and 285E”, *Chem. Commun.*, pp. 1214–1215, 2002.

92. Davison, E. C., M. E. Fox, A. B. Holmes, S. D. Roughley, C. J. Smith, G. M. Williams, J. E. Davies, P. R. Raithby, J. P. Adams, I. T. Forbes, N. J. Press and M. J. Thompson, “Nitrone Dipolar Cycloaddition Routes to Piperidines and Indolizidines. Part 9. Formal Synthesis of (-)-Pinidine and Total Synthesis of (+)-Histrionicotoxin, (-)-Histrionicotoxin and (-)-Histrionicotoxin 235A”, *J. Chem. Soc., Perkin Trans. 1*, pp. 1494–1514, 2002.

93. Horsley, H. T., A. B. Holmes, J. E. Davies, J. M. Goodman, M. A. Silva, S. I. Pascu and I. Collins, “Nitrone Dipolar Cycloaddition Routes to Piperidines and Indolizidines Part 10 - Investigation of Conjugate Addition/Intramolecular Nitrone Dipolar Cycloadditions and Their Use in the Synthesis of Dendrobatid Alkaloid Precursors”, *Org. Biomol. Chem.*, Vol. 2, pp. 1258–1265, 2004.

94. Brasholz, M., J. M. Macdonald, S. Saubern, J. H. Ryan and A. B. Holmes, “A Gram-Scale Batch and Flow Total Synthesis of Perhydrohistrionicotoxin”, *Chem. Eur. J.*, Vol. 16, pp. 11471–11480, 2010.

95. Brasholz, M., B. A. Johnson, J. M. Macdonald, A. Polyzos, J. Tsanaktsidis, S. Saubern, A. B. Holmes and J. H. Ryan, "Flow Synthesis of Tricyclic Spiropiperidines as Building Blocks for the Histrionicotoxin Family of Alkaloids", *Tetrahedron*, Vol. 66, pp. 6445–6449, 2010.

96. Tufariello, J. J. and E. J. Trybulski, "Synthetic Approach to the Skeleton of Histrionicotoxin", *J. Org. Chem.*, Vol. 39, pp. 3378-3384, 1974.

97. Gössinger, E., R. Imhof and H.-U. Wehrli, "Experimental Models in Histrionicotoxin Series - Synthesis of (+/-)-Cis-1-Azaspirol [5.5] Undecan-8-Ols", *Helv. Chim. Acta*, Vol. 58, pp. 96-103, 1975.